New Methods article for Limnology and Oceanography: Methods

Headwater gas exchange quantified from O_2 mass balances at the reach scale

L. Rovelli, [1,2,*] K. M. Attard, [2,3] C. M. Heppell, [4] A. Binley, [5] M. Trimmer, [6] and R. N. Glud, [1,7]

[1] Scottish Marine Institute, Scottish Association for Marine Sciences, PA37 1QA Oban, United Kingdom

[2] Nordcee, Department of Biology, University of Southern Denmark, 5230 Odense M, Denmark

[3] Tvärminne Zoological Station, University of Helsinki, 10900 Hanko, Finland

[4] School of Geography, Queen Mary University of London, Mile End Road, E1 4NS London, United Kingdom

[5] Lancaster Environment Centre, Lancaster University, LA1 4YQ Lancaster, United Kingdom

[6] The School of Biological and Chemical Sciences Queen Mary University of London, E1 4NS London, United Kingdom

[7] Department of Ocean and Environmental Sciences, Tokyo University of Marine Science and Technology, 4-5-7 Konan, Minato-ku, 108-8477 Tokyo, Japan

* corresponding author

Keywords: k, k_2, aquatic eddy co-variance, O_2 budget, open water method

Running title: Reach-scale headwater O_2 gas exchange

Abstract

Headwater streams are important in the carbon cycle and there is a need to better parametrize and quantify exchange of carbon-relevant gases. Thus, we characterized variability in the gas exchange coefficient (k_2) and dissolved oxygen (O_2) gas transfer velocity (k) in two lowland headwaters of the River Avon (UK). The traditional one-station open-water method was complemented by in situ quantification of riverine sources and sinks of O_2 (i.e., groundwater inflow, photosynthesis and respiration in both the water column and benthic compartment) enabling direct hourly estimates of k_2 at the reach–scale (~150 m) without relying on the nighttime regression method. Obtained k_2 values ranged from 0.001 – 0.600 h^{-1}. Average daytime k_2 were a factor two higher than values at night, likely due to diel changes in water temperature and wind. Temperature contributed up to 46% of the variability in k on an hourly scale, but clustering temperature incrementally strengthened the statistical relationship. Our analysis suggested that k variability is aligned with dominant temperature trends rather than with short-term changes. Similarly, wind correlation with k increased when clustering wind speeds in increments correspondent with dominant variations (1 m s^{-1}). Time scale is thus an important consideration when resolving physical drivers of gas exchange. Mean estimates of k_{600} from recent parametrizations proposed for upscaling, when applied to the settings of this study, were found to be in agreement with our independent O_2 budget assessment (within <15%), adding further support to the validity of upscaling efforts aiming at quantifying large-scale riverine gas emissions.

Introduction

Revisions of the global carbon cycle have indicated that rivers and other inland waters contribute substantially to the global cycling of organic carbon and emission of carbon dioxide (CO_2) and methane (CH_4) to the atmosphere (e.g., Cole et al. 2007; Battin et al. 2008; Tranvik et al. 2009; Aufdenkampe et al. 2011; Raymond et al. 2013; Hotchkiss et al. 2015; Stanley et al. 2015; Marx et al. 2017). However, due to a lack of an appropriate universal scaling for quantification of emissions, headwaters (stream order < 4) were initially not included in these assessments (*see* Cole et al. 2007), despite the fact they represent 17% of global riverine area (in perennial riverine systems e.g., Downing et al. 2012). Later inclusions of headwaters have proposed that small streams (order 1) might represent more than a third of the total regional emissions of CO_2 from riverine systems (Butman and Raymond 2011) and thus could be more prominent at the global scale (Raymond et al. 2013). This has highlighted the need for better constraining gas exchange at the reach scale (Trimmer et al. 2012), with the overarching goal of fine-tuning parametrizations used for large scale and global upscaling of metabolism and gas emissions.

Accurate assessments of gas exchange require quantification of the gas transfer velocity, or piston velocity (*k;* unit of length per unit of time^{-1}, e.g., m h^{-1}), which physically controls the exchange of gases at the stream–air interface (*see* Hall et al. 2012). Thus, estimates of *k* are critical to the assessment of emission of greenhouse gases such as CO_2 (e.g., Hotchkiss et al. 2015; Marx et al. 2017) and CH_4 (e.g., Stanley 2015; Crawford and Stanley 2016) and for the quantification of the gas exchange rate of dissolved oxygen (O_2) and estimates of whole-reach metabolism (e.g., Odum 1956). Stream gas exchange is most commonly assessed from total, i.e., whole-stream, metabolism estimates using open water (*OW*) methods based on local

dissolved oxygen (O_2) mass balances (e.g., Odum 1956; Marzolf et al. 1994; Mulholland et al. 2001; Riley and Dodds 2013; Siders et al. 2017). The OW approach provides an integrative quantification of gas exchange R_{ex} (in µmol L^{-1} unit of $time^{-1}$) as

$$R_{ex} = k_2(O_{2(sat)} - O_2) \quad (1)$$

with ($O_{2(sat)}$ - O_2) being the O_2 saturation deficit, i.e., the difference between the O_2 concentration at saturation for the local physical conditions ($O_{2(sat)}$) and the actual O_2 concentration in the stream water, and k_2 the O_2 gas exchange coefficient, often termed the re-aeration coefficient (k_2 or K, unit of $time^{-1}$, e.g., h^{-1}). The coefficient k_2 represents the product of the depth-corrected O_2 gas transfer velocity, or piston velocity (k; unit of length per unit of $time^{-1}$, e.g., m h^{-1}) and local stream area-to-volume ratio, which is often approximated as the inverse of the mean water depth (in m^{-1}) (*see* Raymond et al. 2012; Demars et al. 2015). As assessments of gas exchange critically rely on the quantification of k_2 or k, several direct and indirect methods have been developed for deriving these values.

Direct measurements of these parameters are characterized by the de-gassing of a conservative tracer gas that is subsequently scaled to O_2 (e.g., Wanninkhof et al. 1990; Genereux and Hemond 1992; Reid et al. 2007; Benson et al. 2014). This approach is logistically demanding and temporal upscaling is difficult (Demars et al. 2015). Indirect measurements depend on parameterizations of the local physical characteristics of the stream reach such as depth, flow and slope (e.g., Parker and Gay 1987; Parker and DeSimone 1992 and references therein), as well as fitting of gas transfer parameters to O_2 time series based on simplified relationships (Hornberger and Kelly 1975; Chapra and DiToro 1991; McBride and Chapra 2005) or more complex modeling efforts (Holtgrieve et al. 2010; Grace et al. 2015; Appling et al.

2018). Empirical equations and parameterizations have proven to be useful as predictors of gas-exchange dynamics for specific reaches (*see* Genereux and Hemond 1992), but usually show large discrepancies in k_2 estimates when applied to streams with comparable hydrological characteristics (Moog and Jirka 1998; Aristegi et al. 2009; Palumbo and Brown 2014). To further constrain these parametrizations for spatial upscaling, recent studies have focused on a better characterization of the stream morphology. For example, Raymond et al. (2012) used a large collection of stream metadata to more rigorously scale *k* parametrizations to stream physical characteristics (i.e., flow, depth, slope, discharge).

Although *k* variability on short timescales, i.e., hours, has been reported (e.g., Tobias et al. 2009; Berg and Pace 2017), direct and indirect methods mostly focus on determining a mean value for k_2 for either the day or night, or an average for the whole day-night period, with little consideration being given to its short-term dynamics that are characteristic of most rivers. Recent application of the aquatic eddy co-variance technique (AEC) in rivers has provided robust assessment of reach-scale (~150 m) benthic metabolism (Koopmans and Berg 2015; Rovelli et al. 2017) and, most recently, an 'inverted' AEC approach has been used to directly quantify O_2 gas exchange in large (order 3) streams (Berg and Pace 2017) and in an estuarine embayment (Long and Nicholson 2018). Yet, irrespective of the approach being applied to assess *k*, little emphasis has been given to small headwaters streams (order 1-2), despite their potential implications for the regional and global carbon cycling (e.g., Butman and Raymond 2011; Raymond et al. 2013).

The goal of our study was to provide a proof-of-concept for the derivation (values and dynamics) of k_2 and *k* at the reach scale in small, headwater streams (stream order 1). This was achieved by combining in situ O_2 measurements from a

121 single station OW approach together with direct assessments of riverine metabolism
122 using AEC, sample incubations, and groundwater inflow measurements. The
123 proposed method was compared to the traditional nighttime regression (NR) method,
124 and was used to characterize temporal variability in *k* on hourly to daily time scales.
125 Furthermore, we evaluate *k* dynamics and its relation to the local physical drivers
126 such as mean stream flow, temperature and wind patterns. The results of this study are
127 discussed in light of parametrizations of *k* for regional to large-scale upscaling.
128

Materials and procedures

Study site

This study focused on two headwaters of the Hampshire River Avon, southern England: the Chalk River Ebble (CE) and the Greensand West Avon (GA) (*see* Heppel et al. 2017; Supporting Information Fig. 1). For each headwater, a representative ~150 m reach was selected based on previous surveys of the sub-catchment morphology and geology (*see* field measurements). The selected CE reach (CE1[1]; 51° 1' 41.171" N / 1° 54' 56.309" W) was investigated over three days (25-27 Apr 2013) in spring, when the reach was characterized by a net outflow of stream water to the aquifer, i.e., a losing reach (*see* Supporting Information Fig. 2). The reach was also characterized by profuse growth (36% cover by area) of *Ranunculus spp,* which is widespread throughout the sub-catchment (Watson 1987). The water column of the River Ebble was characterized by low turbidity, with suspended sediment concentration limited to, on average, 37 mg L^{-1} (Heppell and Binley 2016a). The selected GA reach (GA2; 51° 19' 10.173" N / 1° 51' 33.135" W) was investigated over three days from 28-30 Apr 2013. In contrast to the CE reach, the GA reach was characterized by a constant inflow of low-oxygenated groundwater; i.e., a gaining reach (Supporting Information Fig. 2) and only patchy macrophyte coverage (4% by area). Turbidity in the water column was 40% higher on average than at the CE reach (Heppell and Binley 2016a). The reaches are referred to as CE and GA throughout the text.

Reach scale oxygen budget

[1] Reach designations within the Macronutrient Cycles Programme (http://macronutrient-cycles.ouce.ox.ac.uk/).

152 The assessment of O_2 gas exchange and stream metabolism based on a single
153 station open-water approach (e.g., Odum 1956) relies on O_2 time series. Temporal
154 changes in O_2 concentration, dO_2/dt, are attributed to local whole-stream primary
155 production (P), respiration (R) and atmospheric exchange (R_{ex}) as

$$\frac{dO_2}{dt} = P + R + R_{ex} = P + R + k_2(O_{2(sat)} - O_2) \quad (2)$$

156 with k_2 being the gas exchange coefficient (in h^{-1}) and $(O_{2(sat)} - O_2)$ the O_2
157 saturation deficit. The spatial integration of a one-station approach, i.e., the integrated
158 stretch length along the stream, is typically in the order of 1000s of m and can be
159 quantify as $3v/k_2$,with v being the mean stream flow velocity (in m d^{-1}) and k_2 (in d^{-1})(*see* Grace and Imberger 2006).
161 Rates for R and R_{ex} are typically estimated by applying the established
162 nighttime regression (NR) method (Hornberger and Kelly 1975). The method plots
163 the nighttime dO_2/dt at each time step against the O_2 saturation deficit during the
164 night and assumes $P = 0$ and that respiration is light-independent. The resulting linear
165 relationship, obtained via least-squares regression, provides both k_2 (slope) and R
166 (intercept). As NR-based k_2, k_{NR}, is only obtained at night, many studies have adopted
167 a temperature correction term to account for temperature changes between night and
168 day following the parameterization of Elmore and West (1961):

$$k_{2(T)} = k_{2(20°C)}(1.0241)^{(T-20)} \quad (3)$$

169 where $k_{2(20°C)}$ is the gas exchange coefficient at 20°C and $k_{2(T)}$ the gas exchange
170 coefficient at the given temperature T.
171 The O_2 budget (OB) approach used in the current study expands Eq. 2 by
172 accounting for all relevant processes including i) metabolic activity in both sediment

and water, and ii) exchange with both the atmosphere and groundwater (Fig. 1). The temporal O_2 concentration was thus defined as:

$$\frac{dO_2}{dt} = \frac{A}{V}[F_B + F_{WC} + F_K] \quad (4)$$

where F_B, F_{WC}, F_K are the O_2 flux (in mmol m^{-2} h^{-1}) associated with the benthic compartment, the water column, and atmospheric exchange, respectively. The O_2 fluxes were expressed as volumetric rates (in µmol L^{-1} h^{-1}) by multiplying the values by the average ratio between stream area (A) and stream volume (V), which, under smooth stream water surface conditions, is approximated as the mean stream depth (*d*) (Demars et al. 2015).

The main strength of the proposed approach is that each flux component within the OB (Eq. 4) can be directly quantified in the field. Estimates of F_B were obtained from Aquatic Eddy Co-variance (AEC) measurements, while F_{WC} was quantified by incubating discrete water samples in situ (*see* section 2.3). While F_B does include both streambed ($F_{streambed}$) and groundwater contributions to the O_2 budget, fluxes associated with the inflow of O_2 depleted groundwater were independently quantified as:

$$F_{GW} = v_{gw}(O_{2(gw)} - O_2) \quad (5)$$

with $O_{2(gw)}$ being the groundwater O_2 concentration (in µmol L^{-1}), O_2 the in-stream concentration and v_{gw} the local groundwater inflow (in m h^{-1}).

The atmospheric exchange rate was quantified as:

$$F_K = \frac{V}{A}k_2(O_{2(sat)} - O_2) \quad (6)$$

with $k = k_2(V/A) \approx k_2 d$ being the O_2 gas transfer velocity, or O_2 piston velocity (in m h^{-1}) and $O_{2(sat)}$ the local O_2 concentration at saturation. As $O_{2(sat)}$ can be quantified as a

193 function of temperature (*see* Garcia and Gordon 1992), the OB approach effectively
194 enabled a direct estimate of k_2.

195 To facilitate comparisons with published reference values and
196 parameterizations from previous studies, k_2 values were also expressed as $k_{2(20°C)}$ (*see*
197 Eq. 3). Similarly, estimates of O_2 gas transfer velocity were also standardized to a
198 Schmidt number of 600[2] (k_{600}) based on Jahne et al. (1998) as

$$\frac{k_{600}}{k} = \left(\frac{600}{Sc_T}\right)^{-1/2} \quad (7)$$

199 where $Sc_T \approx 0.00086842T^4 - 0.10115T^3 + 4.8055T^2 - 124.34T + 1745.1$ is the
200 Schmidt number for O_2 in freshwater at the local water temperature T (*see*
201 Wanninkhof 2014). Stream temperature time series were obtained from background
202 measurements of physical parameters during the observational period at each site
203 (Rovelli et al. 2016b).
204
205 Field measurements
206 *Site selection* – The investigated reaches (CE and GA) were carefully selected
207 to represent the sub-catchment dominant stream morphology features (e.g., stream
208 course shape, depth, bends, riparian zone) and in-stream habitat patchiness
209 (macrophytes, sediment type). Particular emphasis was given to ensure that each
210 reach also fulfilled the theoretical requirements of the NR method, i.e., streams with
211 relatively high metabolic activity and low gas exchange (*see* Hornberger and Kelly
212 1975). Field measurements were also executed under stable hydrological condition,
213 i.e., constant flow and mean water depth over ≥ 3 days. This enabled i) the evaluation
214 of our local O_2 budget (OB) method and ii) comparisons with the nighttime regression

[2] Schmidt number for CO_2 at 20 °C and O_2 at 17.5 °C in freshwater.

(NR) method and standardized functional equations for k_2 quantification from mean hydrological parameters (Table 4).

Background physicochemical measurements – Stream water column O_2 concentration, temperature and photosynthetically active radiation (PAR) at the streambed (~15 cm above the bottom) were monitored within each reach at 1 min intervals with a conductivity–temperature–depth logger (CTD; XR-420, RBR, Kanata, Canada), equipped with an Aanderraa O_2 optode sensor (Aanderaa, Bergen, Norway) and a 4π PAR sensor (QCP-2000; Biospherical Instruments, San Diego, United States). The data were also used to calibrate the O_2 sensors used for flux estimates and to define nighttime periods (PAR < 2 µmol quanta m^{-2} s^{-1}). Wind speed and direction near the stream surface (1.5 m elevation) were recorded at 15 s intervals with a SkyWatch GEOS 11 portable weather station (JDC Electronic SA, Yverdon-les-Bains, Switzerland).

Benthic oxygen flux – The benthic oxygen flux was quantified using the AEC technique (Berg et al. 2003). Our AEC module consisted of small, lightweight, stainless steel tripod frame equipped with an acoustic Doppler velocimeter (ADV; Vector, Nortek A/S, Rud, Norway), Clark-type O_2 microelectrodes (Revsbech 1989) and submersible O_2 amperometric amplifiers (McGinnis et al. 2011). Up to two O_2 microelectrodes were positioned ~0.5 cm outside the ADV sampling volume, at an inclination of ~60º. Each microelectrode had a 90 % response times < 0.5 s and stirring sensitivity < 0.5 % (Gundersen et al. 1998). The ADV's flow measurements were obtained at 8 – 15 cm from the streambed with a frequency of 64 Hz and with the ADV x-axis aligned to the main flow direction. The acquired datasets were processed following the same procedure described in Rovelli et al. (2017). In short, the dataset was averaged to 8 Hz while applying data quality controls and despiking

routines (e.g., Mori et al. 2007) to the dataset to remove dataset artifacts and reduce signal noise. A double coordinate rotation was applied to the flow time series to minimize the influence of horizontal motions on the vertical velocity component. The datasets were then aligned, i.e., time-shifted, to account for the relative distance between the ADV sampling volume and the microelectrode tip and for the microelectrode time constant (*see* Donis et al. 2015). The AEC-based turbulent oxygen fluxes (in mmol m^{-2} h^{-1}) were estimated from time-averaged vertical velocity fluctuations (w') and O_2 concentration fluctuations (C'), as

$$F_{AEC} = \overline{w'C'} \quad (8)$$

(*see* Berg et al. 2003) via a Reynolds' decomposition, specifically linear detrending, using the program suite Sulfide-Oxygen-Heat Flux Eddy Analysis (SOHFEA version 2.0; *see* McGinnis et al. 2014). The optimal detrending interval represents a trade-off between including low-frequency turbulent contributions and excluding non-turbulent contributions (McGinnis et al. 2008), and was inferred to be 5 min from cumulative averages of oxygen fluxes and friction velocity (u_*) (*see* Attard et al. 2014). To account for the effect of transient O_2 concentration changes in the water column between the sediment-water interface and the AEC measurement height (h), which can potentially bias F_{AEC} (*see* Holtappels et al. 2013; Rheuban et al. 2014), an O_2 storage term was estimated after Rheuban et al. (2014). The benthic oxygen flux corrected for O_2 storage, F_B, was defined as

$$F_B = F_{AEC} + F_{storage} = F_{AEC} + \int_0^h \frac{dC}{dt} dz \quad (9)$$

with dC/dt being the measured O_2 concentration gradient.

The smallest area of the streambed that contributes to 90 % of AEC flux, termed the "footprint area", was estimated from the sediment surface roughness parameter (z_0)

and h following the parameterization by Berg et al. (2007). Values for z_0 were approximated as $z_0 = h \cdot \exp(-\kappa \cdot \frac{u}{u_*})$ with ϰ being the von Karman constant (0.41), and u the average flow velocity (Wüest and Lorke 2003).

Water column activity – Water column oxygen production and consumption rates were estimated by incubating 100 mL rack-mounted glass bottles in situ over 24 h in the light and in the dark, with continuous measurements of O_2 concentration via O_2 optical fibers (4 channel FirestingO2; Pyro Science GmbH, Aachen, Germany). A set of 1 dark bottle, and 1 clear bottle were incubated at the streambed, while 1 bottle was incubated near the stream surface. The fourth bottle was either incubated at mid-depth at GA (depth > 0.4 m) or near the surface for the shallower CE. Three additional replicate sets were also mounted on the rack but O_2 measurements were only performed at the start and end of each incubation via Winkler titrations (Winkler 1888). Volumetric oxygen fluxes (in µmol L^{-1} h^{-1}) were estimated from temporal O_2 concentration gradients via linear regressions for daytime and nighttime periods, respectively. No difference in fluxes were observed at the different depths, indicating a homogenously, well-irradiated water column and thus depth-independent rates. The areal oxygen fluxes F_{WC} (in mmol m^{-2} h^{-1}) were obtained by multiplying the values with the average stream depth. Contributions from macrophytes were deemed to be well-integrated within benthic measurements and thus were not further addressed within the water column oxygen budget (Rovelli et al. 2017).

Groundwater influx – Dissolved oxygen flux resulting from local inflow of O_2 depleted groundwater was estimated based on measurements of the local hydraulic gradients from in-stream piezometers and porewater O_2 concentrations. Two clusters of in-stream piezometers were installed at each site, approximately 10 m apart in the river thalweg. Each cluster comprised three piezometers screened at 20, 50 and 100

cm depth; the 100 cm piezometer was also fitted with narrow polytetrafluoroethylene tubing to depths of 10, 20, 30, 50, 70 and 100 cm for the purposes of pore water sampling. Installation and design of the piezometers followed the description in Binley et al. (2013).

Hydraulic head was measured in all piezometers using HOBO pressure transducers (Onset Computer Corporation, Bourne, United States) at GA and Levelogger Edge pressure transducers (Solinst, Georgetown, Canada) at CE. Measurements were validated with manual dips on a fortnightly basis and, if needed, corrected assuming a linear drift. River stage was measured using a pressure transducer suspended within a stilling well. Falling and rising head slug tests (measurements taken by pressure transducers installed inside the piezometers) were used for computation of saturated hydraulic conductivity using the Hvorslev method (e.g., Binley et al. 2013). Vertical groundwater flux was computed using Darcy's Law, from measurements of the hydraulic gradient between the 50 cm deep piezometric head and local stream stage, combined with a weighted harmonic mean of hydraulic conductivity from slug tests carried out in the 20 cm and 50 cm deep piezometers (*see* Binley et al. 2013).

Pore water samples were collected from sampling tubes located on the piezometers every two months, from February 2014 to June 2016, using a syringe and tygon tubing. The O_2 concentration of pore water and river water was measured immediately following sample collection using a calibrated Clark-type O_2 microelectrode (50 µm tip) connected to an in-line amplifier and data-logging meter (Unisense, Aarhus, Denmark) (*see* Heppell and Binley 2016b).

Data handling – Collected hydrological and physicochemical data were used to i) characterize average conditions at each reach and ii) assess short term, i.e.,

312 hourly, to diel dynamics. O_2 fluxes obtained for each stream compartment were
313 considered separately, to assess their magnitude and variability within and across the
314 reaches, as well as within the O_2 budget context, to quantify and characterize *k*
315 variability.
316

317 **Assessment**

318 Reach characterization

319 Hydrological data and background information for each reach are summarized
320 in Table 1. Temperature ranged from 7.8 – 13.5 °C overall, reflecting a moderate
321 variation (< 5%) between day and night at the two sites. Daily-integrated PAR
322 (PAR_{24}) ranged between 11.9 – 17.4 mol quanta m^{-2} d^{-1}, with peaks of up to 1630
323 µmol quanta m^{-2} s^{-1}. Overall, the average stream flow, based on ADV measurements
324 (12 cm above the streambed), was in the order of 0.18 – 0.33 m s^{-1} with an associated
325 discharge of 0.209 – 0.640 m^3 s^{-1} (Table 1) and showed no significant change between
326 day and night, or within the observational period, indicating a stable flow. Wind
327 speeds at CE showed irregular patterns but an overall higher wind speed during the
328 day than at night (Fig. 2). Wind dynamics at GA, in contrast, were markedly diel,
329 with an average wind speed of 2.4 – 3 m s^{-1} during the day and 0 – 0.2 m s^{-1} at night
330 (Fig. 3). At both sites the water column showed well-defined diel fluctuations in O_2
331 concentration, with nighttime under-saturation (down to 82%) and daytime
332 oversaturation (up to 133%), with diel O_2 concentration changes reaching ~147 µmol
333 L^{-1} (Fig. 2, 3). The O_2 saturation deficit ranged from -108 – -96 µmol L^{-1}, during the
334 day, to 43 – 65 µmol L^{-1}, at night. The average deficit over 24h ranged from 2 µmol
335 L^{-1} to an O_2 saturation surplus of 15 µmol L^{-1}.
336
337 Dissolved oxygen budget
338 *Benthic compartment* – Hourly oxygen fluxes for the benthic compartment
339 ranged between -14.0 to 23.0 mmol m^{-2} h^{-1} (Fig. 2, 3). At CE, oxygen fluxes followed
340 a clear diel pattern (Fig. 2), with average daytime rates of 4.2 mmol m^{-2} h^{-1} and
341 nighttime rates of -2.8 mmol m^{-2} h^{-1}. AEC-based benthic fluxes were estimated to

cover a footprint area 26 m long and 1 m wide (~20 m^2), with most of the flux contribution, i.e. the region of maximum flux, located 0.5 m upstream of the AEC sampling point. At GA, a diel pattern in the benthic oxygen fluxes was also observed (Fig. 3). However, both mean fluxes at night and during the day were negative, amounting to -6.2 mmol m^{-2} h^{-1} and -3.0 mmol m^{-2} h^{-1}, respectively. The theoretical footprint area was 80 m long and 1 m wide (~70 m^2) with the region of maximum flux located 2 m upstream of the of the AEC sampling point.

Water column – At CE, metabolic activity in the water column was below detection (< 0.1 µmol L^{-1} h^{-1}) and negligible for the local O_2 budget (Fig. 2). In contrast, in the more turbid, sandy GA, water column activity ranged from net oxygen production rates of 2.8 µmol L^{-1} h^{-1} during the day, to oxygen consumption of -0.9 µmol L^{-1} h^{-1} at night. The average daytime rate of oxygen production was ~1.2 mmol m^{-2} h^{-1}, with an average nighttime consumption rate of -0.5 mmol m^{-2} h^{-1} (Fig. 3).

Groundwater – During our study, the CE reach was losing water to the aquifer. This net local outflow of stream water had no measurable effect on in-stream O_2 concentrations (Fig. 2). At gaining reach GA, the inflow of groundwater amounted to 0.043 m d^{-1} on average, with a mean groundwater O_2 concentration of 63.5 µmol L^{-1}. Groundwater contributed to an areal O_2 concentration decrease of -0.4 – -0.7 mmol m^{-2} h^{-1} (average -0.5 mmol m^{-2} h^{-1}), representing 6-7% of the combined nighttime flux caused by metabolic activity in the benthic compartment and the water column (Fig. 3).

Atmospheric exchange – The derived rate of O_2 exchange between the stream and the atmosphere ranged from -22.3 to 14.5 mmol m^{-2} h^{-1}. Estimates of k_2 based on the O_2 budget (OB) method ranged from 0.001 to 0.600 h^{-1}, with mean values of 0.252 h^{-1} and 0.,259 h^{-1} for CE and GA, respectively (Table 2). Within such range of k_2 and

with mean flow velocities of 0.18 – 0.33 m s^{-1}, one-station based assessment are expected to integrate a stream length of > 7 km).

Estimates of the gas exchange coefficient k_2 using the NR method (k_{NR}) were 0.555 h^{-1} at CE and 0.434 h^{-1} at GA (Table 3 and Supporting Information Fig. 3), and thus around a factor 2 higher than those obtained with the OB method. (Table 2, 3). At CE, we observed a significant ($p < 0.01$) difference between daytime and nighttime estimates of k_2 (Fig. 2 and Table 2). The average daytime k_2 (k_{day}) was 0.331 h^{-1} and about 2 times higher than k_2 at night (k_{night}). Similar conditions were observed at GA (Fig. 3 and Table 2), suggesting that diel changes in temperature and wind could partly explain the observed difference between day and night variability in k_2 at both sites.

Dynamics and variability of O_2 gas exchange

Temperature – Gas exchange coefficient (k_2) and gas transfer velocity (k) are expected to be related to local stream temperature (Elmore and West 1961; Kilpatrick et al. 1989; Demars and Manson 2013). Yet, temperature has been reported to be a weak predictor of k in some settings (Tobias et al. 2009; Demars and Mason 2013), as well as in modeling studies (e.g., Correa-Gonzalez et al. 2014). For example, Tobias et al. (2009) used a modified sulfur hexafluoride (SF_6) tracer approach to assess variability in k (k_{SF6}) on time scales of hours (in 3h intervals) and found that k_{SF6} varied by 30% over a 32 h observational period and could apportion 39% of the observed variability to changes in temperature (Demars and Mason 2013).

At CE, our hourly estimates of k varied by 60%, on average, between consecutive measurements during our 3 days observational period, with temperature accounting for 46% of that variability (Supporting Information Fig. 4). As expected

392 from previous studies (e.g., Tobias et al. 2009; Demars and Manson 2013), part of this
393 variability could be accounted for by applying the Elmore and West (1961)
394 temperature correction to normalize k to 20°C (k_{20}; Supporting Information Fig. 4).
395 However, we found that temperature corrected k_{20} could only explain 10% of the k –
396 temperature relationship, and only 5% of the variability measured in k at CE. This
397 provided further evidence that the dynamics of k could not be properly accounted for
398 by simple functions for temperature corrections.
399 Instead, at CE we found that the relationship between k and temperature could
400 be strengthened by clustering k values to fixed temperature increments, increasing
401 stepwise from 0.5 to 1.7°C. The best linear relationships (i.e., highest regression
402 coefficients) were observed by clustering data in increments of 1.0 to 1.5 °C ($R^2 >$
403 0.8), with R^2 decreasing, either side, for shorter or longer increments (Supporting
404 Information Fig. 4) and we found the best fit to the data occurred with 1.5°C
405 increments (Fig. 4a). As the clustering procedure partially accounts for the variability
406 in both temperature and k, the trend in increasing fit to the data (higher R^2) suggested
407 that dynamics in k and temperature, and their interaction, may occur at variable time
408 scales. This trend was, however, not observed at GA, where temperature revealed no
409 direct correlation with k on hourly time scales (R^2=0.02) or with temperature
410 clustering (R^2=0.03), indicating that temperature changes in the water column did not
411 significantly contribute to k variability at the site.
412 Temperature dynamics, however, may affect gas exchange without any
413 detectable changes in bulk O_2 concentrations in the water, as recently proposed by
414 Berg and Pace (2017). The authors applied the same AEC approach as in this study,
415 but in an "upside-down" configuration, with AEC measurements being performed
416 near the (underside) of the stream surface (~5 cm below the atmosphere-water

417 interface), rather than near the streambed. This enabled the quantification of O_2 flux
418 and heat flux across the stream surface, from which they inferred local O_2 gas
419 exchange and values for *k*. Their results showed that temperature fluctuations
420 occurring just below the surface might bias the quantification of O_2 fluctuations and
421 thus AEC-based assessments of *k*. The implications of the study by Berg and Pace
422 (2017) suggest that other methodological approaches commonly used for the
423 quantification of *k* at timescales ranging from minutes to complete diel cycles could
424 also be impacted. The absence of any relationship between water column temperature
425 and *k* at GA could thus, in part, be attributed to small-scale temperature dynamics that
426 are not accounted for by simple temperature correction functions; though other
427 physical parameters such as wind, for example, could also modulate *k* at GA.
428 *Wind* – Here the reaches were open to the wind (e.g., Supporting Information
429 Fig. 1), with frequent wind-induced ripples being observed during the day, suggesting
430 an interaction between flow and wind that could affect gas exchange. On time scales
431 of hours, however, wind dynamics revealed no significant relationship with the
432 derived variability in *k* (R^2=0.13). Similar results have also been reported from other
433 methodological approaches, e.g., tracer release (Tobias and al. 2009) and AEC (Berg
434 et al. 2017); though both studies relied on off-site, rather than on-site wind
435 measurements. As large variability in both *k* and wind might mask any general trend,
436 wind data were temporally clustered to investigate any time lag between wind
437 dynamics and derived *k* values. Using a bin interval of 1 m s^{-1}, which represented the
438 dominant (> 90%) wind fluctuations at each site (Supporting Information Fig. 5), we
439 revealed a robust positive linear relationship (R^2 > 0.7) between local wind and k_{600} at
440 each site and for both sites combined (Fig. 4b). Given the relatively low range in wind
441 speed (0 – 4 m s^{-1}), a linear relationship provided a suitable approximation, though for

more extensive ranges in wind speed a quadratic form is more appropriate (e.g., Wanninkhof 1992; Nightingale et al. 2000; Sweeney et al. 2007; Wanninkhof 2014). Similarly to the effect of temperature, increasing or decreasing the size of the wind clustering increment resulted in a lowering of the regression coefficient, thus further supporting the argument of a temporal misalignment between the drivers of k variability and actual k dynamics.

Discussion

Parametrization of gas exchange coefficients

Our study was performed under stable discharge and constant stream depth, which allowed both i) the evaluation of our local O_2 budget (OB) method for deriving k_2 directly and then, ii) the comparison with the nighttime regression (NR) method and standardized functional equations for k_2 quantification (Table 4). The advantage of the OB method over the latter approaches is that the method is not limited to stable hydrological conditions or specific time periods. This contrasts with the NR method, for instance, where estimates of k_2 obtained at night might not be applicable during the day. Furthermore, the OB approach relies on in situ measurements of local O_2 mass balance variables, rather than parametrizations and scaling relationship from literature values. The method is therefore ideal for investigating discrepancies between the various procedures for estimating k_2 and thus strengthens the parameterization procedures applied for upscaling global estimates of outgassing coefficients for other gases such as CO_2 and CH_4.

In this study, the NR method systematically provided among the highest estimates of k_2 for both reaches. Values of k_{NR} were, on average, a factor of two higher than k_2 derived by the OB method (Fig. 5). The largest discrepancies, by up to a factor of three, were observed at nighttime, while, during the daytime, mean values were within reported uncertainties for this approach (Palumbo and Brown 2014). Potential issues with NR method applicability or dataset quality were deemed marginal, as both CE and GA met the requirements of the NR method (*see* Methods), and the O_2 time series were of a high quality (Supporting Information Fig. 3). Therefore, the observed discrepancies in k_2 are attributed to a biased estimation of R derived at nighttime using the NR method (R_{NR}), leading to a systematic

overestimation of k_2.

Studies investigating the effect of local inflows of O_2-depleted groundwater have shown that groundwater might bias the quantification of R in open water approaches and thus whole-stream O_2 budget assessments (e.g., McCutchan et al. 2002; Hall and Tank 2005; Koopmans and Berg 2015). The magnitude of such effect, which would lead to an overestimation of R, might vary according to hydrological characteristics and hydrological connectivity of each stream, ranging from negligible to substantial (*see* McCutchan et al. 2002). In this study, the contribution from groundwater to the O_2 budgets was quantified directly. At gaining reach GA, groundwater contributions to whole-stream estimates of R were limited to 0.5 mmol m^{-2} h^{-1}, representing < 5% of the mean R_{NR} (15.5 mmol m^{-2} h^{-1}); the combined R from the benthic compartment and water column activity was 6.7 mmol m^{-2} h^{-1}. At losing reach CE, contributions from groundwater were negligible but the NR method still estimated R at 8.7 mmol m^{-2} h^{-1}, which is some 3-fold higher than our direct measurements (2.8 mmol m^{-2} h^{-1}).

An overestimation of R during night could also result from a temporal misalignment between actual changes in whole stream respiration and physical parameters controlling gas exchange. As shown in both datasets (Fig. 2, 3), temperature decreased at night until about 6 – 8 AM, and directly affected the measured saturation deficit. If k_2 is assumed to be constant, as shown from our NR regression plots (*see* Supporting Information Fig. 3), then the temperature-driven increase in the O_2 concentration at saturation, and associated O_2 saturation deficit, will result in an erroneous estimate of the magnitude of R_{NR}.

It has recently been shown that k (and thus k_2) might display changes of up to a factor of 2–3 over timescales of 10s of minutes to hours, even under constant

hydrological conditions (e.g., Berg and Pace 2017), implying that k_2 will not remain constant over the several hours' time scale associated with the NR method. Since the NR approach considers changes in the magnitude of k_2 as a direct and instantaneous consequence of changes in *R, v*ariability in k_2 could explain the magnitude of the R_{NR} bias obtained in this study, though the drivers of that variability, such as temperature, wind and stream discharge, need further investigation (Berg and Pace 2017).

Hydrological parameters such as stream depth, stream flow and stream energy (e.g., slope, shear velocity) have been used to derive k_2 (e.g., O'Connor and Dobbins 1958; Palumbo and Brown 2014) and subsequently k_{600}. Given the local hydrology (0.4 – 0.57 m mean depth, 0.18 – 0.33 m s^{-1} mean flow velocity), our mean values of k_{600} derived with the (OB) method (0.121 ± 0.007 m h^{-1} for CE and 0.190 ± 0.016 m h^{-1} for GA), are well within the range predicted by 19 sets of proposed functional equations extracted from the literature (0.009 – 0.236 m h^{-1} at CE and 0.023 – 0.373 m h^{-1} at GA; Table 4, Fig. 5). NR-derived values were also within that range, although they ranked towards the upper end of the range. As expected from previous studies (*see* Aristegi et al. 2009; Palumbo and Brown 2014), estimates from each equation were highly scattered throughout the obtained range, with little consistency between the two sites. For instance, even equations that were previously identified to perform well in hydrology settings similar to our study, i.e., "top performer" equations (*see* Palumbo and Brown 2014), still showed large discrepancies - both within and across sites (Fig. 5). In contrast, we found that the revised functional equations provided by Raymond et al. (2012) provided well-constrained estimates, which were not only consistent within sites (*see* Supporting Information Fig. 6), but also between sites, with mean k_{600} values (0.113 m h^{-1} for CE and 0.201 m h^{-1} for GA) within 5–7% of the local estimates from our OB method (Fig. 5).

524

525 **Comments and recommendations**

526 The aquatic eddy co-variance technique (AEC) has been shown to be an
527 effective tool for quantifying streambed metabolism and, more recently, for the
528 quantification of O_2 gas exchange and k from O_2 fluxes near the stream surface (Berg
529 and Pace 2017). A combination of the AEC technique with other traditional methods
530 appears to be a promising next step towards better constrained assessments of gas
531 exchange and k dynamics in headwaters, provided that careful consideration is given
532 to i) the site selection and ii) the representativeness of the reach within the km-sized
533 integration of, e.g., open-water approaches. The O_2 budget (OB) approach presented
534 in this study serves as a proof-of-concept towards this goal. While the approach is
535 more time consuming and field demanding that traditional methods, it does enable i)
536 the compartmentalization of stream metabolism and ii) the assessment of short-term k
537 variability. The study has highlighted short-term variability in k dynamics with a
538 dampened relationship to variations of well-known physical drivers. The apparent
539 lack of correlation could be attributed to temporal misalignments between the
540 variability of the derived k and physical drivers, and to small-scale variability in
541 temperature. This was clearly observed at CE, where temperature-corrected k_{20} and
542 k_{600} values still revealed a marked temperature dependency, suggesting that common
543 temperature corrections were insufficient to fully account for the observed k
544 variability. It remains unclear whether and to what extend such small-scale variability
545 in temperature will affect the overall gas exchange.
546 Although the above aspects are still poorly constrained at the local scale and on short
547 time scales (hours), estimates of k from the most recent functional parametrizations
548 compared well with the independent assessments of this study and should therefore be

549 preferred over earlier parametrizations. Validations of *k* on local scales such as the
550 ones presented in this study are strongly required to strengthen and add more
551 confidence to the upscaling of *k* for the quantification of large-scale metabolism and
552 global emission of climate-relevant gases such as CO_2 and CH_4 across headwaters and
553 throughout riverine networks.

554 **References**

555 Appling, A. P., R. O. Hall, C. B. Yackulic, and M. Arroita. 2018. Overcoming
556 equifinality: leveraging long time series for stream metabolism estimation. J.
557 Geophys. Res. Biogeosciences **123**: 624–645. doi:10.1002/2017JG004140
558 Aristegi, L., O. Izagirre, and A. Elosegi. 2009. Comparison of several methods to
559 calculate reaeration in streams, and their effects on estimation of metabolism.
560 Hydrobiologia **635**: 113–124. doi:10.1007/S10750-009-9904-8
561 Attard, K. M., R. N. Glud, D. F. McGinnis, and S. Rysgaard. 2014. Seasonal rates of
562 benthic primary production in a Greenland fjord measured by aquatic eddy-
563 correlation. Limnol. Oceanogr. **59**: 1555–1569. doi:10.4319/lo.2014.59.5.1555
564 Aufdenkampe, A. K., E. Mayorga, P. A. Raymond, J. M. Melack, S. C. Doney, S. R.
565 Alin, R. E. Aalto, and K. Yoo. 2011. Riverine coupling of biogeochemical
566 cycles between land, oceans, and atmosphere. Front. Ecol. Environ. **9**: 53–60.
567 doi:10.1890/100014
568 Bansal, M. K. 1973. Atmospheric reaeration in natural streams. Water Res. **7**: 769–
569 782. doi:10.1016/0043-1354(73)90092-4
570 Battin, T. J., L. A. Kaplan, S. Findlay, C. S. Hopkinson, E. Marti, A. I. Packman, J. D.
571 Newbold, and F. Sabater. 2008. Biophysical controls on organic carbon fluxes
572 in fluvial networks. Nat. Geosci. **1**: 95–100. doi:10.1038/Ngeo101
573 Bennett, J. P., and R. E. Rathbun. 1972. Reaeration in open-channel flow. U.S.
574 Geological Survey Prof. Pap. 737, U.S. Government Printing Office,
575 Washington, DC.
576 Benson, A., M. Zane, T. E. Becker, A. Visser, S. H. Uriostegui, E. DeRubeis, J. E.
577 Moran, B. K. Esser, and J. F. Clark. 2014. Quantifying Reaeration Rates in
578 Alpine Streams Using Deliberate Gas Tracer Experiments. Water **6**: 1013–
579 1027. doi:10.3390/w6041013
580 Berg, P., H. Røy, F. Janssen, V. Meyer, B. B. Jørgensen, M. Huettel, and D. de Beer.
581 2003. Oxygen uptake by aquatic sediments measured with a novel non-
582 invasive eddy-correlation technique. Mar. Ecol. Progr. Ser. **261**: 75–83.
583 doi:10.3354/meps261075
584 Berg, P., H. Røy, and P. L. Wiberg. 2007. Eddy correlation flux measurements: The
585 sediment surface area that contributes to the flux. Limnol. Oceanogr. **52**: 1672–
586 1684. doi:10.4319/lo.2007.52.4.1672

587 Berg, P., M. L. Delgard, R. N. Glud, M. Huettel, C. E. Reimers, and M. L. Pace.
588 2017. L. Non-invasive flux measurements at the benthic interface: the aquatic
589 eddy covariance technique. Limnol. Oceanogr.: e-lectures **7**: 1–50.
590 doi:10.1002/loe2.10005
591 Berg, P., and M. L. Pace. 2017. Continuous measurement of air-water gas exchange
592 by underwater eddy covariance. Biogeosciences **14**: 5595–5606.
593 doi:10.5194/bg-14-5595-2017
594 Binley, A., S. Ullah, A. L. Heathwaite, C. Heppell, P. Byrne, K. Lansdown, M.
595 Trimmer, and H. Zhang. 2013. Revealing the spatial variability of water fluxes
596 at the groundwater-surface water interface. Water Resour. Res. **49**: 3978–3992.
597 doi:10.1002/wrcr.20214
598 Butman, D., and P. A. Raymond. 2011. Significant efflux of carbon dioxide from
599 streams and rivers in the United States. Nat. Geosci. **4**: 839–842.
600 doi:10.1038/ngeo1294
601 Cadwallader, T. E., and A. J. McDonnell. 1969. A multivariate analysis of reaeration
602 data. Water Res. **3**: 731–742. doi:10.1016/0043-1354(69)90037-2
603 Chapra, S. C., and D. M. DiToro. 1991. Delta method for estimating primary
604 production, respiration, and reaeration in streams. J. Environ. Eng. **117**: 640–
605 655. doi:10.1061/(ASCE)0733-9372(1991)117:5(640)
606 Churchill, M. A.; H. L. Elmore, and R. A. Buckingham. 1962. The prediction of
607 stream reaeration rates. Int. J. Air Water Poll. **6**: 467–467. doi:10.1016/B978-1-
608 4832-8391-3.50015-4
609 Cole, J. J., Y. T. Prairie, N. F. Caraco, W. H. McDowell, L. J. Tranvik, R. G. Striegl,
610 C. M. Duarte, P. Kortelainen, J. A. Downing, J. J. Middelburg, and J. Melack.
611 2007. Plumbing the global carbon cycle: integrating inland waters into the
612 terrestrial carbon budget. Ecosystems **10**: 172–184. doi:10.1007/s10021-006-
613 9013-8
614 Correa-Gonzalez, J. C., M. D. Chavez-Parga, J. A. Cortes, and R. M. Perez-Munguia.
615 2014. Correa-Gonzalez, J. C.; Chavez-Parga, M. D.; Cortes, J. A.; Perez-
616 Munguia, R. M. Photosynthesis, respiration and reaeration in a stream with
617 complex dissolved oxygen pattern and temperature dependence. Ecol. Modell.
618 **273**: 220–227. doi:10.1016/j.ecolmodel.2013.11.018

619 Crawford, J. T., and E. H. Stanley. 2016. Controls on methane concentrations and
620 fluxes in streams draining human-dominated landscapes. Ecol. Appl. **26**: 1581–
621 1591. doi:10.1890/15-1330
622 Demars, B. O. L., and J. R. Manson. 2013. Temperature dependence of stream
623 aeration coefficients and the effect of water turbulence: A critical review.
624 Water Res. **47**: 1–15. doi:10.1016/j.watres.2012.09.054
625 Demars, B. O. L., J. Thompson, and J. R. Manson. 2015. Stream metabolism and the
626 open diel oxygen method: Principles, practice, and perspectives. Limnol.
627 Oceanogr.: Methods **13**: 356–374. doi:10.1002/lom3.10030
628 Dobbins, W. E. 1965. BOD and oxygen relationships in streams. J. Sanit. Eng. Div.
629 **90**(3): 53–78.
630 Donis, D., M. Holtappels, C. Noss, C. Cathalot, K. Hancke, P. Polsenaere, F.
631 Wenzhöfer, A. Lorke, F. J. R. Meysman, R. N. Glud, and D. F. McGinnis.
632 2015. An Assessment of the Precision and Confidence of Aquatic Eddy
633 Correlation Measurements. J. Atmos. Oceanic Technol. **32**: 642–655.
634 doi:10.1175/JTECH-D-14-00089.1
635 Downing, J. A., J. J. Cole, C. M. Duarte, J. J. Middelburg, J. M. Melack, Y. T.
636 Prairie, P. Kortelainen, R. G. Striegl, W. H. McDowell, and L. J. Tranvik.
637 2012. Global abundance and size distribution of streams and rivers. Inland
638 Waters **2**: 229–236. doi:10.5268/Iw-2.4.502
639 Elmore, H. L., and W. F. West. 1961. Effect of water temperature on stream
640 reaeration. J. Sanit. Eng. Div., Am. Soc. Civ. Eng. **87**(SA6): 59–71.
641 Garcia, H. E., and L. I. Gordon. 1992. Oxygen Solubility in Seawater - Better Fitting
642 Equations. Limnol. Oceanogr. **37**: 1307–1312. doi:10.4319/lo.1992.37.6.1307
643 Genereux, D. P., and H. F. Hemond. 1992. Determination of gas exchange rate
644 constants for a small stream on Walker Branch watershed, Tennessee. Water
645 Resour. Res. **28**: 2365–2374. doi:10.1029/92WR01083
646 Grace, M. R., and S. J. Imberger. 2006. Stream metabolism: Performing and
647 interpreting measurements. pp. 204. Water Studies Centre, Monash University.
648 Report for the Murray Darling Basin Commission and the New South Wales
649 Department of Environment and Climate Change.
650 Grace, M. R., D. P. Giling, S. Hladyz, V. Caron, R. M. Thompson, and R. Mac
651 Nally. 2015. Fast processing of diel oxygen curves: Estimating stream
652 metabolism with BASE (BAyesian Single-station Estimation). Limnol.

653 Oceanogr.: Methods **13**: 103–114. doi:10.1002/lom.10011
654 Gundersen, J. K., N. B. Ramsing, and R. N. Glud. 1998. Predicting the signal of O_2
655 microsensors from physical dimensions, temperature, salinity, and O_2
656 concentration. Limnol. Oceanogr. **43**: 1932–1937.
657 doi:10.4319/lo.1998.43.8.1932
658 Hall, R. O., and J. L. Tank. 2005. Correcting whole-stream estimates of metabolism
659 for groundwater input. Limnol. Oceanogr.: Methods **3**: 222–229.
660 doi:10.4319/lom.2005.3.222
661 Hall, R. O., T. A. Kennedy, and E. J. Rosi-Marshall. 2012. Air-water oxygen
662 exchange in a large whitewater river. Limnol. Oceanogr.: Fluids and
663 Environments **2**: 1–11. doi:10.1215/21573689-1572535
664 Heppell, C. M., and A. Binley. 2016a. Hampshire Avon: Daily discharge, stage and
665 water chemistry data from four tributaries (Sem, Nadder, West Avon, Ebble).
666 NERC Environmental Information Data Centre. Available from
667 https://doi.org/10.5285/0dd10858-7b96-41f1-8db5-e7b4c4168af5
668 Heppell, C. M., and A. Binley. 2016b. Vertical head gradient, saturated hydraulic
669 conductivity and pore water chemistry data from six river reaches. NERC
670 Environmental Information Data Centre. Available from
671 https://doi.org/10.5285/d82a04ce-f04d-40b4-9750-1a2bf7dc29a3
672 Heppell, C. M., A. Binley, M. Trimmer, T. Darch, A. Jones, E. Malone, A. L.
673 Collins, P. J. Johnes, J. E. Freer, and C. E. M. Lloyd. 2017. Hydrological
674 controls on DOC: Nitrate resource stoichiometry in a lowland, agricultural
675 catchment, southern UK. Hydrol. Earth Syst. Sci. **21**: 4785–4802.
676 doi:10.5194/hess-21-4785-2017
677 Holtappels, M., R. N. Glud, D. Donis, B. Liu, A. Hume, F. Wenzhöfer, and M. M.
678 M. Kuypers. 2013. Effects of transient bottom water currents and oxygen
679 concentrations on benthic exchange rates as assessed by eddy correlation
680 measurements. J. Geophys. Res.: Oceans **118**: 1157–1169.
681 doi:10.1002/jgrc.20112
682 Holtgrieve, G. W., D. E. Schindler, T. A. Branch, and Z. T. A'mar. 2010.
683 Simultaneous quantification of aquatic ecosystem metabolism and reaeration
684 using a Bayesian statistical model of oxygen dynamics. Limnol. Oceanogr. **55**:
685 1047–1063. doi:10.4319/lo.2010.55.3.1047

686 Hornberger, G. M., and M. G. Kelly. 1975. Atmospheric reaeration in a river using
687 productivity analysis. J. Environ. Eng. Div. **101**(5): 729–739.
688 Hotchkiss, E. R., R. O. Hall, R. A. Sponseller, D. Butman, J. Klaminder, H. Laudon,
689 M. Rosvall, and J. Karlsson. 2015. Sources of and processes controlling CO_2
690 emissions change with the size of streams and rivers. Nat. Geosci. **8**: 696–699.
691 doi:10.1038/ngeo2507
692 Isaacs, W. P., A. F. Gaudy Jr. 1968. Atmospheric oxygenation in a simulated stream.
693 J. Sanit. Eng. Div. **94**(2): 319–344.
694 Jahne, B., K. O. Munnich, R. Bosinger, A. Dutzi, and W. Huber. 1987. On
695 parameters influencing air-water gas exchange. J. Geophys. Res. **74**: 456–464.
696 doi:10.1029/JC092iC02p01937
697 Kilpatrick, F. A., R. E. Rathbun, N. Yotsukura, G. W. Parker, and L. L. DeLong.
698 1989. Determination of stream reaeration coefficients by use of tracers. Page
699 52 Techniques of water-resources investigations 3-A18. U.S. Geological
700 Survey, Denver, Colorado.
701 Koopmans, D., and P. Berg. 2015. Stream oxygen flux and metabolism determined
702 with the open water and eddy correlation techniques. Limnol. Oceanogr. **60**:
703 1344–1355. doi:10.1002/lno.10103
704 Krenkel, P. A., and G. T. Orlob. 1963. Turbulent diffusion and the reaeration
705 coefficient. J. Sanit. Eng. Div. **88**(2): 53–83.
706 Langbein, W. B., and W. H. Durum. 1967. The aeration capacity of streams. USGS
707 Circ. S42, USGS, Washington, DC.
708 Long, M. H., and D. P. Nicholson. 2018. Surface gas exchange determined from an
709 aquatic eddy covariance floating platform. Limnol. Oceanogr. Methods **16**:
710 145–159. doi:10.1002/lom3.10233
711 Marx, A., J. Dusek, J. Jankovec, M. Sanda, T. Vogel, R. van Geldern, J. Hartmann,
712 and J. A. C. Barth. 2017. A review of CO_2 and associated carbon dynamics in
713 headwater streams: A global perspective. Rev. Geophys. **55**: 560–585.
714 doi:10.1002/2016RG000547
715 Marzolf, E. R., P. J. Mulholland, and A. D. Steinman. 1994. Improvements to the
716 Diurnal Upstream-Downstream Dissolved-Oxygen Change Technique for
717 Determining Whole-Stream Metabolism in Small Streams. Can. J. Fish. Aquat.
718 Sci. **51**: 1591–1599. doi:10.1139/F94-158
719 McBride, G. B., and S.C. Chapra. 2005. Rapid calculation of oxygen in streams:

720 approximate delta method. J. Environ. Eng. **131**: 336–342.
721 doi:10.1061/(ASCE)0733-9372(2005)131:3(336)
722 McCutchan, J. H., J. F. Saunders, W. M. Lewis, and M. G. Hayden. 2002. Effects of
723 groundwater flux on open-channel estimates of stream metabolism. Limnol.
724 Oceanogr. **47**: 321–324. doi:10.4319/lo.2002.47.1.0321
725 McGinnis, D. F., P. Berg, A. Brand, C. Lorrai, T. J. Edmonds, and A. Wüest. 2008.
726 Measurements of eddy correlation oxygen fluxes in shallow freshwaters:
727 Towards routine applications and analysis. Geophys. Res. Lett. **35**: L04403.
728 doi:10.1029/2007GL032747
729 McGinnis, D. F., S. Cherednichenko, S. Sommer, P. Berg, L. Rovelli, R. Schwarz, R.
730 N. Glud, and P. Linke. 2011. Simple, robust eddy correlation amplifier for
731 aquatic dissolved oxygen and hydrogen sulfide flux measurements. Limnol.
732 Oceanogr.: Methods **9**: 340–347. doi:10.4319/lom.2011.9.340
733 McGinnis, D. F., S. Sommer, A. Lorke, R. N. Glud, and P. Linke. 2014. Quantifying
734 tidally driven benthic oxygen exchange across permeable sediments: An
735 aquatic eddy correlation study. J. Geophys. Res.: Oceans **119**: 6918–6932.
736 doi:10.1002/2014JC010303
737 Moog, D. B., and G. H. Jirka. 1998. Analysis of reaeration equations using mean
738 multiplicative error. J. Environ. Eng. **124**: 104–110. doi:10.1061/(ASCE)0733-
739 9372(1998)124:2(104)
740 Mori, N., T. Suzuki, and S. Kakuno. 2007. Noise of acoustic Doppler velocimeter
741 data in bubbly flow. J. Eng. Mech. **133**: 122–125. doi:10.1061/(ASCE)0733-
742 9399(2007)133:1(122)
743 Mulholland, P. J., C. S. Fellows, J. L. Tank, N. B. Grimm, J. R. Webster, S. K.
744 Hamilton, E. Marti, L. Ashkenas, W. B. Bowden, W. K. Dodds, W. H.
745 McDowell, M. J. Paul, and B. J. Peterson. 2001. Inter-biome comparison of
746 factors controlling stream metabolism. Freshwater Biol. **46**: 1503–1517.
747 doi:10.1046/j.1365-2427.2001.00773.x
748 Negulescu, M., and V. Rojanski. 1969. Recent research to determine reaeration
749 coefficient. Water Res. **3**: 189–192. doi:10.1016/0043-1354(69)90058-X
750 Nightingale, P. D., G. Malin, C. S. Law, A. J. Watson, P. S. Liss, M. I. Liddicoat, J.
751 Boutin, and R. C. Upstill-Goddard. 2000. In situ evaluation of air-sea gas
752 exchange parameterizations using novel conservative and volatile tracers.
753 Global Biogeochem. Cycles **14**: 373–387. doi:10.1029/1999gb900091

O'Connor, D. J., and W. E. Dobbins. 1958. Mechanism of reaeration in natural streams. Am. Soc. Civ. Eng. **123**(1): 641–684.

Odum, H. T. 1956. Primary Production in Flowing Waters. Limnol. Oceanogr. **1**: 102–117. doi:10.4319/lo.1956.1.2.0102

Owens, M., R. W. Edwards, and J. W. Gibbs. 1964. Some reaeration studies in streams. Int. J. Air Water Pollut. **8**: 469–486.

Owens, M. 1974. Measurement on non-isolated natural com- munities in running waters. *In* R. A. Vollenweider [ed.], A manual on methods for measuring primary production in aquatic environments. Blackwell Scientific, Oxford, United Kingdom.

Padden, T. J., and E. F. Gloyna. 1971. Simulation of stream processes in a model river. Rep. No. EHE-70-23, University of Texas, Austin, TX.

Palumbo, J. E., and L. C. Brown. 2014. Assessing the performance of reaeration prediction equations. J. Environ. Eng. **140**: 04013013. doi:10.1061/(ASCE)EE.1943-7870.0000799

Parkhurst, J. D., and R. D. Pomeroy. 1972. Oxygen absorption in streams. J. Sanit. Eng. Div. **98**(1): 101–124.

Parker, G. W., and F. B. Gay. 1987. A procedure for estimating reaeration coefficients for Massachusetts streams. U.S. Geological Survey. Water Resources Invest. Rep. 86- 4111. USGS, Reston, VA.

Parker, G. W., and L. A. DeSimone. 1992. Estimating reaeration coefficients for low-slope streams in Massachusetts and New York, 1985-88. U.S. Geological Survey, Water Resources Invest. Rep. 91-4188, USGS, Washington, DC.

Raymond, P. A., C. J. Zappa, D. Butman, T. L. Bott, J. Potter, P. Mulholland, A. E. Laursen, W. H. McDowell, and D. Newbold. 2012. Scaling the gas transfer velocity and hydraulic geometry in streams and small rivers. Limnol. Oceanogr.: Fluids and Environments **2**: 41–53. doi:10.1215/21573689-1597669

Raymond, P. A., J. Hartmann, R. Lauerwald, S. Sobek, C. McDonald, M. Hoover, D. Butman, R. Striegl, E. Mayorga, C. Humborg, P. Kortelainen, H. Durr, M. Meybeck, P. Ciais, and P. Guth. 2013. Global carbon dioxide emissions from inland waters. Nature **503**: 355–359. doi:10.1038/nature12760

Revsbech, N. P. 1989. An oxygen microelectrode with a guard cathode. Limnol. Oceanogr. **34**: 474–478. doi:10.4319/lo.1989.34.2.0474

788 Rheuban, J. E., P. Berg, and K. J. McGlathery. 2014. Multiple timescale processes
789 drive ecosystem metabolism in eelgrass (Zostera marina) meadows. Mar. Ecol.
790 Progr. Ser. **507**: 1–13. doi:10.3354/Meps10843
791 Riley, A. J., and W. K. Dodds. 2013. Whole-stream metabolism: strategies for
792 measuring and modeling diel trends of dissolved oxygen. Freshw. Sci. **32**: 56–
793 69. doi:10.1899/12-058.1
794 Reid, S. E., P. A. Mackinnon, and T. Elliot. 2007. Direct measurements of reaeration
795 rates using noble gas tracers in the River Lagan, Northern Ireland. Water
796 Environ. J. **21**: 182–191. doi:10.1111/j.1747-6593.2007.00069.x
797 Rovelli, L., K. M. Attard, A. Binley, C. M. Heppell, H. Stahl, M. Trimmer, and R. N.
798 Glud. 2017. Reach-scale river metabolism across contrasting sub-catchment
799 geologies: Effect of light and hydrology. Limnol. Oceanogr. **62**: S381–S399.
800 doi:10.1002/lno.10619
801 Rovelli, L., K. M. Attard, H. Stahl, and R. N. Glud. **2016**a Flow velocity transects
802 collected seasonally at six tributaries of Hampshire River Avon from 2013 to
803 2014. NERC Environmental Information Data Centre. Available from
804 https://doi.org/10.5285/16df35a9-90ab-4273-8b6c-5ef3648ec76d
805 Rovelli, L., K. M. Attard, H. Stahl, and R. N. Glud. **2016b.** In situ near-streambed
806 light regime and water column dissolved oxygen and temperature measurements
807 performed seasonally at six tributaries of Hampshire River Avon from 2013 to
808 2014. NERC Environmental Information Data Centre. Available from
809 https://doi.org/10.5285/c1f14c54-ffe1-4581-b479-897ff9262e98
810 Smoot, J. L. 1988. An examination of stream reaeration coefficients and hydraulic
811 conditions in a pool-and-riffle stream. Ph.D. Dissertation, Virginia Polytechnic
812 Institute and State University, Blacksburg, VA.
813 Siders, A. C., D. M. Larson, J. Ruegg, and W. K. Dodds. 2017. Probing whole-
814 stream metabolism: influence of spatial heterogeneity on rate estimates.
815 Freshwater Biol. **62**: 711–723. doi:10.1111/fwb.12896
816 Stanley, E. H., N. J. Casson, S. T. Christel, J. T. Crawford, L. C. Loken, and S. K.
817 Oliver. 2016. The ecology of methane in streams and rivers: patterns, controls,
818 and global significance. Ecol. Monogr. **86**: 146–171. doi:10.1890/15-1027.1
819 Sweeney, C., E. Gloor, A. R. Jacobson, R. M. Key, G. McKinley, J. L. Sarmiento, and
820 R. Wanninkhof. 2007. Constraining global air-sea gas exchange for CO_2 with

recent bomb ^{14}C measurements. Global Biogeochem. Cycles **21**: Gb2015. doi:10.1029/2006gb002784

Tobias, C. R., J. K. Bohlke, J. W. Harvey, and E. Busenberg. 2009. A simple technique for continuous measurement of time-variable gas transfer in surface waters. Limnol. Oceanogr.: Methods **7**: 185–195. doi:10.4319/lom.2009.7

Thackston, E. L., and P. A. Krenkel. 1969. Reaeration prediction in natural streams. J. Sanit. Eng. Div. **95**: 65–94.

Thackston, E. L., and J. W. Dawson. 2001. Recalibration of a reaeration equation. J. Environ. Eng. **127**: 317–321. doi:10.1061/(ASCE)0733-9372(2001)127:4(317)

Tranvik, L. J., J. A. Downing, J. B. Cotner, S. A. Loiselle, R. G. Striegl, T. J. Ballatore, P. Dillon, K. Finlay, K. Fortino, L. B. Knoll, P. L. Kortelainen, T. Kutser, S. Larsen, I. Laurion, D. M. Leech, S. L. McCallister, D. M. McKnight, J. M. Melack, E. Overholt, J. A. Porter, Y. T. Prairie, W. H. Renwick, F. Roland, B. S. Sherman, D. W. Schindler, S. Sobek, A. Tremblay, M. J. Vanni, A. M. Verschoor, E. von Wachenfeldt, and G. A. Weyhenmeyer. 2009. Lakes and reservoirs as regulators of carbon cycling and climate. Limnol. Oceanogr. **54**: 2298–2314. doi:10.4319/lo.2009.54.6_part_2.2298

Trimmer, M., J. Grey, C. M. Heppell, A. G. Hildrew, K. Lansdown, H. Stahl, and G. Yvon-Durocher. 2012. River bed carbon and nitrogen cycling: State of play and some new directions. Sci. Total Environ. **434**: 143–158. doi:10.1016/j.scitotenv.2011.10.074

Tsivoglou, E. C., and L. A. Neal. 1976. Tracer measurement of reaeration: 3. Predicting the reaeration capacity of inland streams. J. Water Pollut. Control Fed **48**: 2669–2689.

Wanninkhof, R., P. J. Mulholland, and J. W. Elwood. 1990. Gas exchange rates for a first-order stream determined with deliberate and natural tracers. Water Resour. Res. **26**: 1621–1630. doi:10.1029/WR026i007p01621

Wanninkhof, R. 1992. Relationship between wind speed and gas exchange over the ocean. J. Geophys. Res. **97**: 7373–7382. doi:10.1029/92JC00188

Wanninkhof, R. 2014. Relationship between wind speed and gas exchange over the ocean revisited. Limnol. Oceanogr.: Methods **12**: 351–362. doi:10.4319/lom.2014.12.351

Watson, D. 1987. Hydraulic effects of aquatic weeds in U.K. rivers. Regulated Rivers: Research & Management **1**(3): 211–227. doi:10.1002/rrr.3450010303

855 Winkler, L. 1888. Die Bestimmung des in Wasser gelösten Sauerstoffes. Ber. Dtsch.
856 Chem. Ges. 21: 2843–2855. doi:10.1002/cber.188802102122
857 Wüest, A., and A. Lorke. 2003. Small-scale hydrodynamics in lakes. Annu. Rev.
858 Fluid Mech. **35**: 373–412. doi:10.1146/annurev.fluid.35.101101.161220
859

Acknowledgments

We are grateful to the stakeholders of the National Environmental Research Council (NERC) Macronutrient Cycles programme for their support (grants NE/J012106/1 awarded to MT, NE/J011681/1 awarded to RNG, and NE/J011738/1 awarded to AB). We thank Henrik Stahl for his valuable support during the planning and execution of the field measurements, and Katrina Lansdown, Louise Olde, Kasper Hancke, Christopher McCaig, and John Montgomery, for their support and company during field work. We are grateful to Anni Glud for providing O_2 electrodes and optodes for this study, to Ashley Jones and Edward Malone for collecting and summarizing the catchments' hydrological data. We also thank Dirk Koopmans and two anonymous reviewers for their constructive reviews of this work.

This study contributes to the project HADES-ERC funded by the European Research Council Advanced Investigator Grant 669947. This project has received funding from the European Union's Horizon 2020 research and innovation programme under grant agreement No 678760 (ATLAS). This output reflects only the author's view and the European Union cannot be held responsible for any use that may be made of the information contained therein. LR, KMA, KA, and RNG and CMH received financial support from NERC—NE/F018614/1, NE/F012691/1, NE/J011681/1, NE/J012106/1; The Commission for Scientific Research in Greenland (KVUG)— GCRC6507; The Danish Council for Independent Research (FNU-12-125843); ERC Advanced Grant, ERC-2010-AdG_20100224 and the Danish National Research Foundation (DRNF53).

Figure Legends

Fig. 1. Dissolved oxygen mass balance approach. Changes in stream O_2 concentration are expressed as a function of contributions from the water column (F_{WC}), benthic compartment (F_B) and atmospheric exchange (F_K) following the parameterization of Eq. 4. Benthic F_B includes contributions from the streambed ($F_{streambed}$) and from groundwater inflow/outflow (F_{GW}). Note that lateral exchange and advection processes were not considered.

Fig. 2. Estimates of k_2 for the river Ebble (CE) during the spring. (A) Wind speed recorded 1.5 m above the stream surface. (B) Local dissolved oxygen (O_2) concentration (gray line) and associated O_2 concentration at atmospheric saturation (dotted line). Black lines indicate nighttime (PAR < 2 µmol quanta m^{-2} s^{-1}). (C) Time series of oxygen fluxes encompassing benthic (F_B), water column (F_{WC}) and groundwater (F_{GW}) contributions to the local O_2 budget. (D) Hourly averaged estimates of k_2 based on the O_2 budget (OB) method in spring (circles), with temperature overlain (dashed line).

Fig. 3. Estimates of k_2 for the river West Avon (GA) during the spring. (A) Wind speed recorded 1.5 m above the stream surface. (B) Local dissolved oxygen (O_2) concentration (gray line) and associated O_2 concentration at atmospheric saturation (dotted line). Black lines indicate nighttime (PAR < 2 µmol quanta m^{-2} s^{-1}). (C) Time series of oxygen fluxes encompassing benthic (F_B), water column (F_{WC}) and groundwater (F_{GW}) contributions to the local O_2 budget. (D) Hourly averaged estimates of k_2 based on the O_2 budget (OB) method in spring (circles), with temperature overlain (solid line). Note that the wind data were shifted by 24 h to fill the measurement gap on day 1.

Fig. 4. Temperature and wind dependencies of the gas transfer velocity k. (A) Temperature relationship of k at CE. Values for k (solid black circles), k normalized to 20°C (k_{20}; open grey circles) and to a Schmidt number of 600 (k_{600}, solid grey circles) were clustered into 1.5°C temperature increments to account for temporal misalignments and to provide the most robust linear analysis ($R^2 > 0.9$; *see* Supporting Information Fig. 4). (B) Standardized k_{600} as a function of wind speed for CE (solid black squares), GA (open white squares) and both sites combined (dotted line). Wind speeds were clustered into 1 m s^{-1} bins to account for the dominant

917 magnitude of wind fluctuations (*see* Supporting Information Fig. 5). Linear trends
918 were obtained via least squares regression.
919
920 Fig. 5. Estimates of k_{600} (in m h^{-1}) for (A) river Ebble and (B) West Avon. Estimates are
921 obtained from different published hydrological parameterizations (Equations 1 – 18, and
922 Raymond et al. (2012)); from the O_2 budget (OB) method used in this study (*see* Eq. 4); and
923 from the nighttime regression (NR) method. Equation numbering follows Table 4. Note that
924 crossed equations were reported to be the "top-performer" within a specific mean depth and
925 mean flow range from an extensive database of tracer-based k_2 values and hydrological
926 parameters (*see* Palumbo and Brown 2014). Mean value and uncertainty range (dashed and
927 dotted lines) for the hydrological parameterizations of Raymond et al. (2012) were obtained
928 by combining mean and range from of each equation. (*see* Table 4; Supporting Information
929 Fig. 6). Note that to better highlight the differences between the OB, NR and common
930 parametrizations, the equation order was re-arranged to show an incremental increase in k_{600}.
931

926 **Tables**

927 Table 1. Summary of hydrological and physicochemical data for river Ebble (CE) and West Avon (GA). Average values are presented as mean ±
928 standard error. Values between square brackets indicate the range of the measurements.

Site	Period	Daylight [h]	Total PAR [mol m^{-2} d^{-1}]	O_2 [% sat]	O_2 [µmol L^{-1}]	T [°C]	Depth[1] [m]	Width[1] [m]	Flow [m s^{-1}]	Discharge[1] [m^3 s^{-1}]
CE	25-27 Apr 2013	15.3	11.9	106.6 ± 0.3 [87.7 – 132.7]	367.7 ± 0.9 [301.5 – 449.5]	10.8 ± 0.03 [8.4 – 13.5]	0.41	5.25	0.18	0.640
GA	28-30 Apr 2013	15.3	17.4	101.5 ± 0.3 [82.3 – 127.2]	365.3 ± 1.2 [303.0 – 449.3]	9.0 ± 0.02 [7.8 – 10.7]	0.57	2.75	0.33	0.385

929 1: Obtained from depth and flow velocity transects performed during the observational period under stable hydrograph (*see* Rovelli et al. 2016a).

930 Table 2. Estimates of k_2 (in h^{-1}) using the O_2 budget (OB) method. Values for daytime, nighttime and average over the observational period are
931 reported as mean ± standard error, with *n* indicating the number of averaged data points. Standardized $k_{2(20°C)}$ (in h^{-1}) and k_{600} (in m h^{-1}) are also
932 reported to enable better comparisons with literature studies.

Site	Day	Night	Mean
		k_2 [h^{-1}] (*n*)	
CE	0.331 ± 0.024 (63)	0.170 ± 0.012 (62)	0.252 ± 0.015 (125)
GA	0.367 ± 0.034 (26)	0.188 ± 0.020 (37)	0.261 ± 0.021 (63)
		$k_{2(20°C)}$ [h^{-1}] (*n*)	
CE	0.404 ± 0.030 (63)	0.214 ± 0.014 (62)	0.310 ± 0.019 (125)
GA	0.478 ± 0.045 (26)	0.248 ± 0.027 (37)	0.343 ± 0.028 (63)
		k_{600} [m h^{-1}] (*n*)	
CE	0.157 ± 0.012 (63)	0.084 ± 0.006 (62)	0.121 ± 0.007 (125)
GA	0.265 ± 0.025 (26)	0.137 ± 0.015 (37)	0.190 ± 0.016 (63)

933
934

Table 3. Estimates of k_2 using the nighttime regression method (k_{NR}). Values are reported with the respective regression coefficient (R^2) for each site. The associated plots are available in the Supporting Information (Fig. 3). The temperature-normalized values of k_{NR} for 20 °C ($k_{NR(20°C)}$), are computed based on the mean nighttime temperature at each site, while the daily NR-based k scaled for a Schmidt number of 600 ($k_{NR(600)}$, in m h^{-1}) was computed for the mean daily temperatures.

Site	k_{NR} [h^{-1}] (R^2)	$k_{NR(20°C)}$ [h^{-1}]	$k_{NR(600)}$ [m h^{-1}]	Night temperature (°C)
CE	0.554 (0.78)	0.694	0.273	10.5
GA	0.421 (0.78)	0.539	0.304	8.7

940 Table 4. Estimates of k_{600} (in m h^{-1}) from established empirical equations applied to the CE and GA study sites. Input variables[#]: d – stream
941 depth (m), u – flow velocity (m s^{-1}), u^* – friction velocity (m s^{-1}), s – stream slope (m m^{-1}), Q – discharge (m^3 s^{-1}), and $Fr = u/\sqrt{gd}$ – Froude
942 number with g being the gravitational acceleration constant. Note that most equations provide k_2 at 20°C ($k_{2(20°C)}$, in day^{-1}; Supporting
943 Information Table 1); $k_{2(20°C)}$ values that were scaled to k_{600} based on Eq.7 and the O_2 Schmidt number for 20°C (Table 1).

Eq.	Reference	Abbr.[##]	Equations	CE k_{600} [m h^{-1}]	GA k_{600} [m h^{-1}]
1	O'Connor and Dobbins (1958)	OD	$k_{2(20°C)} = 3.9\frac{u^{0.5}}{d^{1.5}}$	0.099	0.114
2a	Churchill et al. (1962)	E_4	$k_{2(20°C)} = 0.0217\frac{u^{2.695}}{d^{3.085}s^{0.825}}$	0.009	0.023
2b		CEB	$k_{2(20°C)} = 5.01\frac{u^{0.969}}{d^{1.673}}$	0.067	0.096
3	Krenkel and Orlob (1963)	E_6, KO	$k_{2(20°C)} = 173.01\frac{(us)^{0.404}}{d^{0.66}}$	0.199	0.285
4a	Owens et al. (1964)	E_8	$k_{2(20°C)} = 6.91\frac{u^{0.73}}{d^{1.75}}$	0.148	0.180
4b		E_9, OEG	$k_{2(20°C)} = 5.35\frac{u^{0.67}}{d^{1.85}}$	0.139	0.158
5	Dobbins (1965)	DB*	$k_{2(20°C)} = 55.2\frac{1+Fr^2}{(0.9+Fr)^{1.5}}\frac{(us)^{0.375}}{d}\coth\left[\frac{4.75(us)^{0.125}}{(0.9+Fr)^{0.5}}\right]$	0.117	0.139
6a	Langbein and Durum (1967)	E_7	$k_{2(20°C)} = 5.14\frac{u}{d^{1.33}}$	0.048	0.078
6b		LD	$k_{2(20°C)} = 5.14\frac{u}{d^{0.67}}$	0.026	0.054
7	Issacs and Gaudy (1968)	IG	$k_{2(20°C)} = 4.76\frac{u}{d^{1.5}}$	0.051	0.080
8	Cadwallader and McDonnell (1969)	E_3, CM	$k_{2(20°C)} = 186.07\frac{(us)^{0.5}}{d}$	0.136	0.184

9	Negulescu and Rojanski (1969)	NR	$k_{2(20°C)} = 10.91\left(\frac{u}{d}\right)^{0.85}$	0.085	0.150
10	Thackston and Krenkel (1969)	TK*	$k_{2(20°C)} = 24.9\frac{u^*(1+Fr^{0.5})}{d}$	0.013	0.025
11	Padden and Gloyna (1971)	PG	$k_{2(20°C)} = 4.53\frac{u^{0.703}}{d^{1.054}}$	0.055	0.082
12a	Bennett and Rathbun (1972)	E_1, BR1	$k_{2(20°C)} = 32.69\frac{u^{0.413}s^{0.273}}{d^{1.408}}$	0.163	0.183
12b		E_2, BR2	$k_{2(20°C)} = 5.58\frac{u^{0.607}}{d^{1.689}}$	0.140	0.161
13	Parkhurst and Pomeroy (1972)	PP*	$k_{2(20°C)} = 48.5\frac{(1+0.17Fr^2)(us)^{0.375}}{d}$	0.097	0.122
14	Bansal (1973)	BN	$k_{2(20°C)} = 1.81\frac{u^{0.6}}{d^{1.4}}$	0.036	0.045
15	Owens (1974)	–	$k_{2(20°C)} = 50.8\frac{u^{0.67}}{d^{0.85}}^{###}$	0.236	0.373
16	Tsivoglou and Neal (1976)	E_{10}, TN	$k_{2(20°C)} = k_2'us^{####}$	0.128	0.325
17	Smoot (1988)	SM	$k_{2(20°C)} = 543\frac{u^{0.5325}s^{0.6236}}{d^{0.7258}}$	0.136	0.206
18	Thackston and Dawson (2001)	TD*	$k_{2(20°C)} = 4.97\frac{u^*(1+9Fr^{0.25})}{d}$	0.012	0.024
19a	Raymond et al. (2012)	Rm_1	$k_{600} = 5037(us)^{0.89}d^{0.54}$	0.113	0.231
19b		Rm_2	$k_{600} = 5937(1-2.54Fr^2)(us)^{0.89}d^{0.58}$	0.125	0.252
19c		Rm_3	$k_{600} = 1162u^{0.85}s^{0.77}$	0.096	0.160
19d		Rm_4	$k_{600} = 951.5(us)^{0.76}$	0.097	0.154
19e		Rm_5	$k_{600} = 2841us + 2.02$	0.127	0.162
19f		Rm_6	$k_{600} = 929(us)^{0.75}Q^{0.011}$	0.102	0.160
19g		Rm_7	$k_{600} = 4725(us)^{0.86}Q^{-0.14}d^{0.66}$	0.128	0.287

944 #: Average stream depth and flow velocity are taken from (Table 1). The average shear velocity, u_*, computed as $u_* = u(C_D)^{1/2}$, with C_D being the drag coefficient (Wüest and
945 Lorke 2003). An average C_D of 3.3 x 10^{-3} was used for both sites based on further surveys of the River Avon sub-catchments (Rovelli et al. 2017). The average slope, 0.002 m m^{-1},
946 was estimated from GPS measurements during the respective field campaigns.
947 ##: Reference equation numbers and abbreviations from Aristegi et al. (2009) and Palumbo and Brown (2014), respectively.
948 ###: This equation requires depth in cm and flow velocity in cm s^{-1}.
949 ####: with k_2' being 31183 s m^{-1} d^{-1} for Q < 0.280 m^3 s^{-1} and 22500 s m^{-1} d^{-1} for Q > 0.280 m^3 s^{-1}, respectively (Palumbo and Brown 2014).
950 *: These equations were identified to be the most suited (i.e., top performer) for the site mean depth and flow based on the suggestions of Palumbo and Brown (2014).

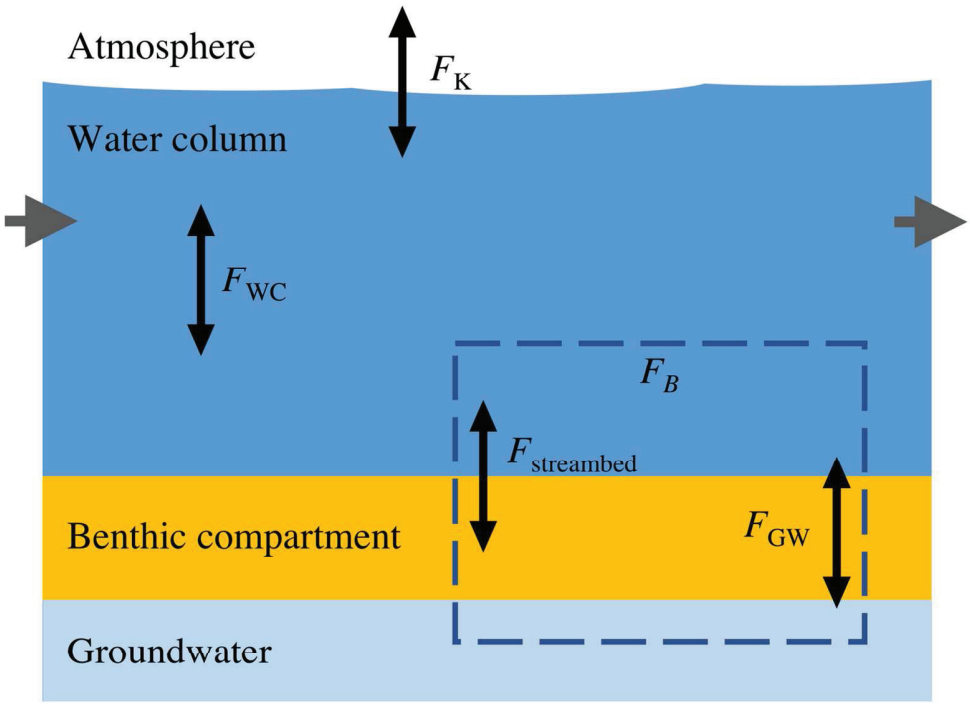

Figure 1. Dissolved oxygen mass balance approach. Changes in stream O_2 concentration are expressed as a function of contributions from the water column (F_{WC}), benthic compartment (F_B) and atmospheric exchange (F_K) following the parameterization of Eq. 4. Benthic F_B includes contributions from the streambed ($F_{streambed}$) and from groundwater inflow/outflow (F_{GW}). Note that lateral exchange and advection processes were not considered.

69x54mm (600 x 600 DPI)

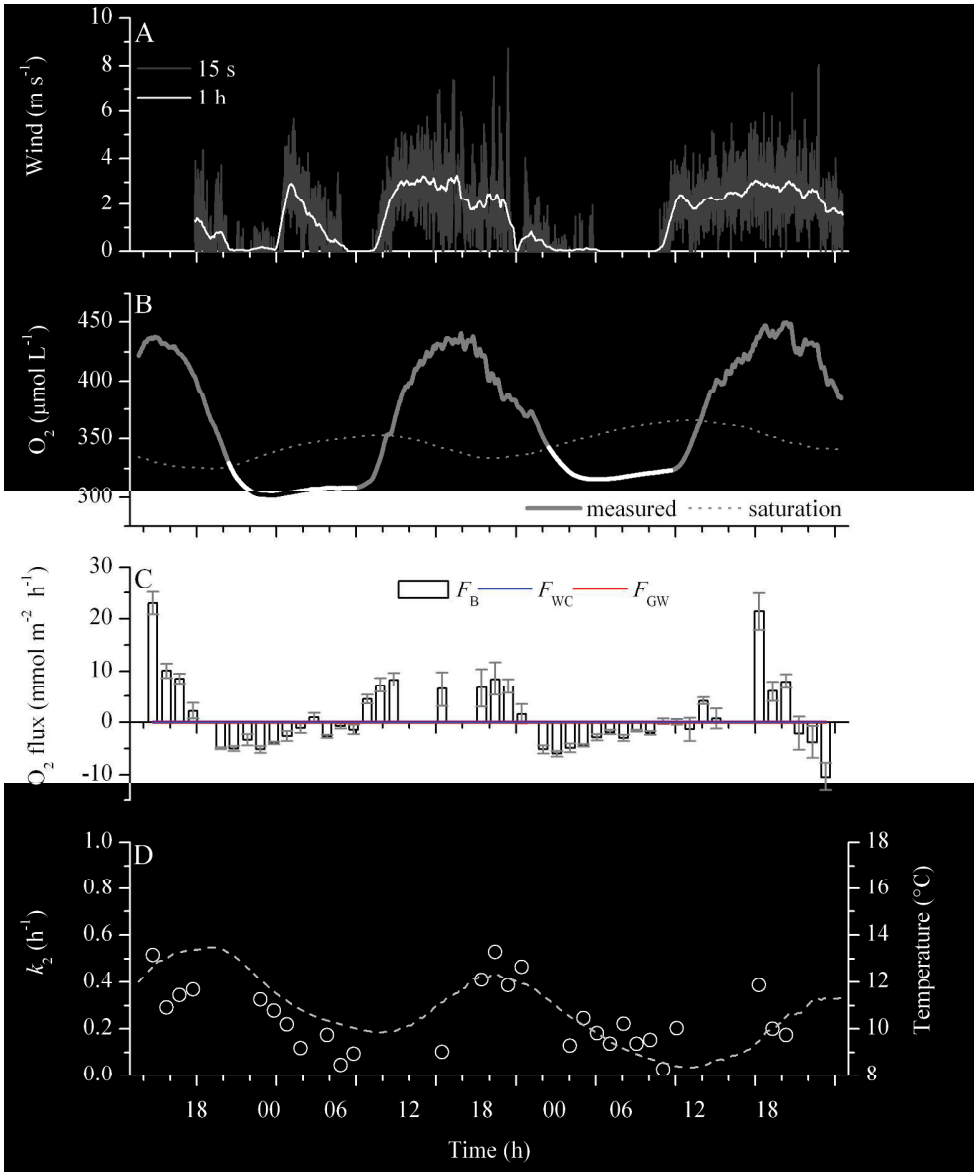

Figure 2. Estimates of k_2 for the river Ebble (CE) during spring. (A) Wind speed recorded 1.5 m above the stream surface. (B) Local dissolved oxygen (O_2) concentration (gray line) and associated O_2 concentration at atmospheric saturation (dotted line). Black lines indicate nighttime (PAR < 2 µmol quanta m^{-2} s^{-1}). (C) Time series of oxygen fluxes encompassing benthic (F_B), water column (F_{WC}) and groundwater (F_{GW}) contributions to the local O_2 budget. (D) Hourly averaged estimates of k_2 based on the O_2 budget (OB) method in spring (circles), with temperature overlain (dashed line).

532x640mm (150 x 150 DPI)

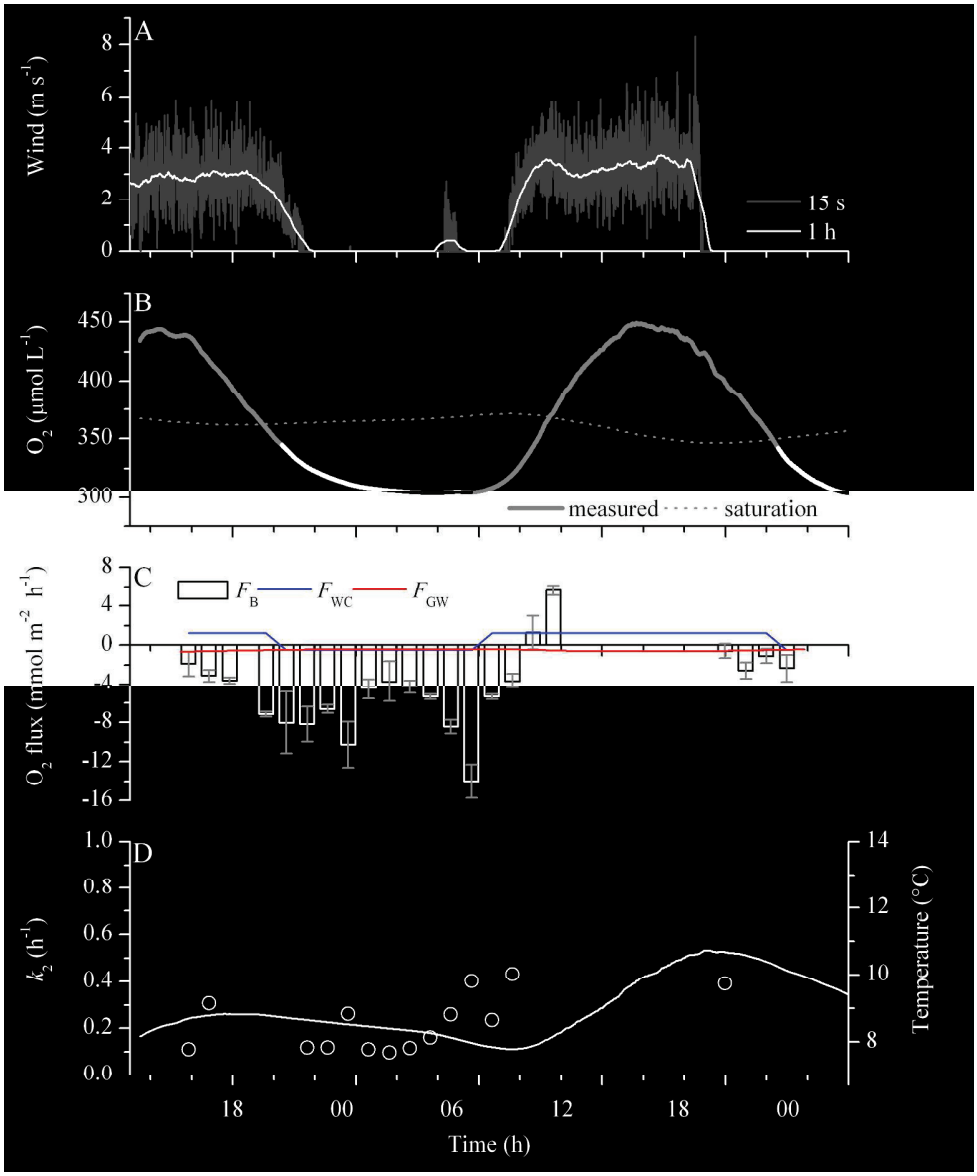

Figure 3. Estimates of k_2 for the river West Avon (GA) during the spring. (A) Wind speed recorded 1.5 m above the stream surface. (B) Local dissolved oxygen (O_2) concentration (gray line) and associated O_2 concentration at atmospheric saturation (dotted line). Black lines indicate nighttime (PAR < 2 µmol quanta m^{-2} s^{-1}). (C) Time series of oxygen fluxes encompassing benthic (F_B), water column (F_{WC}) and groundwater (F_{GW}) contributions to the local O_2 budget. (D) Hourly averaged estimates of k_2 based on the O_2 budget (OB) method in spring (circles), with temperature overlain (solid line). Note that the wind data were shifted by 24 h to fill the measurement gap on day 1.

532x640mm (150 x 150 DPI)

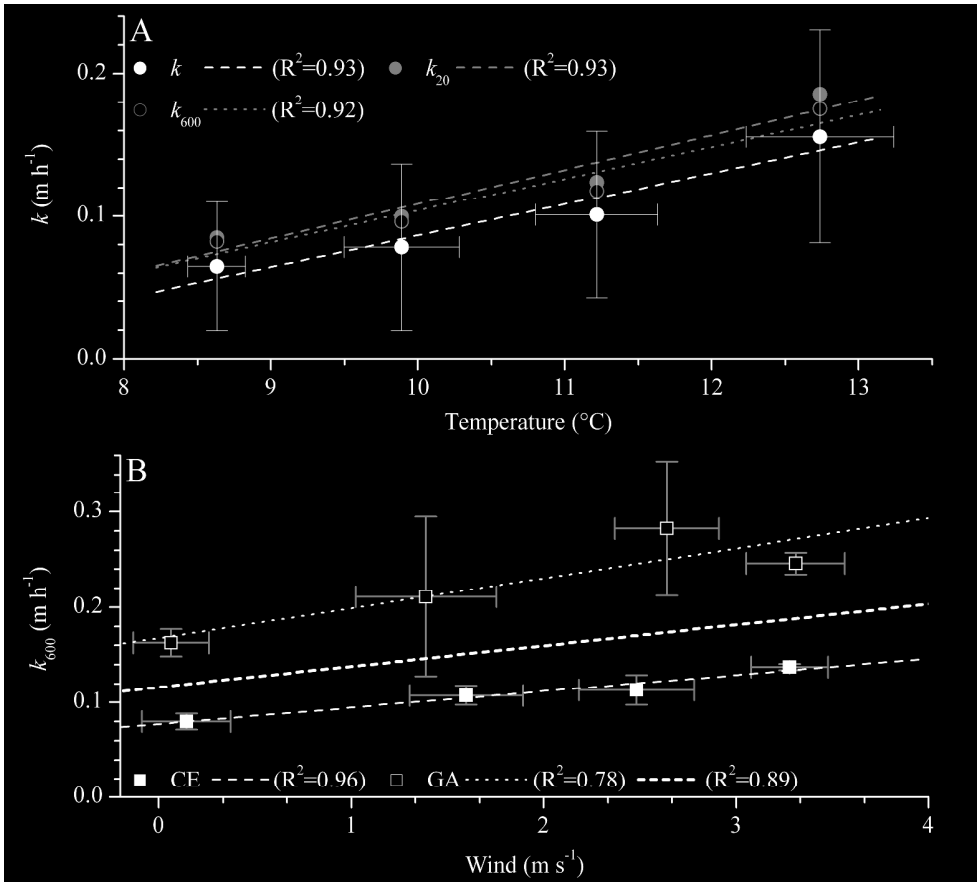

Figure 4. Temperature and wind dependencies of the gas transfer velocity *k*. (A) Temperature relationship of *k* at CE. Values for *k* (solid black circles), *k* normalized to 20°C (k_{20}; open grey circles) and to a Schmidt number of 600 (k_{600}, solid grey circles) were clustered into 1.5°C temperature increments to account for temporal misalignments and to provide the most robust linear analysis ($R^2 > 0.9$; *see* Supporting Information Fig. 4). (B) Standardized k_{600} as a function of wind speed for CE (solid black squares), GA (open white squares) and both sites combined (dotted line). Wind speeds were clustered into 1 m s^{-1} bins to account for the dominant magnitude of wind fluctuations (*see* Supporting Information Fig. 5). Linear trends were obtained via least squares regression.

1064x959mm (150 x 150 DPI)

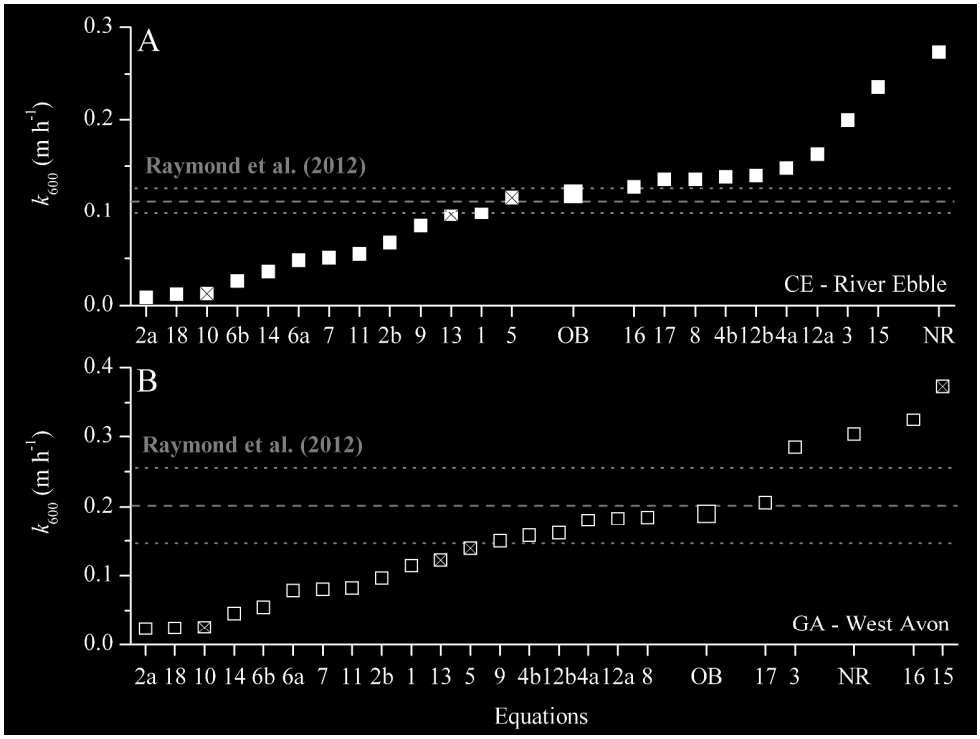

Figure 5. Estimates of k_{600} (in m h^{-1}) for (A) river Ebble and (B) West Avon. Estimates are obtained from different published hydrological parameterizations (Equations 1 — 18, and Raymond et al. (2012)); from the O_2 budget (OB) method used in this study (*see* Eq. 4); and from the nighttime regression (NR) method. Equation numbering follows Table 4. Note that crossed equations were reported to be the "top-performer" within a specific mean depth and mean flow range from an extensive database of tracer-based k_2 values and hydrological parameters (*see* Palumbo and Brown 2014). Mean value and uncertainty range (dashed and dotted lines) for the hydrological parameterizations of Raymond et al. (2012) were obtained by combining mean and range from of each equation. (*see* Table 4; Supporting Information Fig. 6). Note that to better highlight the differences between the OB, NR and common parametrizations, the equation order was re-arranged to show an incremental increase in k_{600}.

1064x799mm (150 x 150 DPI)

Supporting information for

Headwater gas exchange quantified from O_2 mass balances at the reach scale

L. Rovelli, [1,2,*] K. M. Attard, [2,3] C. M. Heppell, [4] A. Binley, [5] M. Trimmer, [6] and R. N. Glud, [1,7]

[1] Scottish Marine Institute, Scottish Association for Marine Sciences, PA37 1QA Oban, United Kingdom

[2] Nordcee, Department of Biology, University of Southern Denmark, 5230 Odense M, Denmark

[3] Tvärminne Zoological Station, University of Helsinki, 10900 Hanko, Finland

[4] School of Geography, Queen Mary University of London, Mile End Road, E1 4NS London, United Kingdom

[5] Lancaster Environment Centre, Lancaster University, LA1 4YQ Lancaster, United Kingdom

[6] The School of Biological and Chemical Sciences Queen Mary University of London, E1 4NS London, United Kingdom

[7] Department of Ocean and Environmental Sciences, Tokyo University of Marine Science and Technology, 4-5-7 Konan, Minato-ku, 108-8477 Tokyo, Japan

* corresponding author

10 pages, 1 table, 6 figures

Supporting Tables

Table 4. Estimates of k_2 at 20°C ($k_{2(20°C)}$, in day^{-1}) from established empirical equations applied to the CE and GA study sites. Input variables[#]: d – stream depth (m), u – flow velocity (m s^{-1}), u^* – friction velocity (m s^{-1}), s – stream slope (m m^{-1}), Q – discharge (m^3 s^{-1}), and $Fr = u/\sqrt{gd}$ – Froude number with g being the gravitational acceleration constant. Note that for equations providing k_{600} (in m day^{-1}) $k_{2(20°C)}$ values were scaled based on Eq. 7 and the O_2 Schmidt number at 20°C.

Eq.	Reference	Abbr.[##]	Equations	CE $k_{2(20°C)}$ [day^{-1}]	GA $k_{2(20°C)}$ [day^{-1}]
1	O'Connor and Dobbins (1958)	OD	$k_2 = 3.9\frac{u^{0.5}}{d^{1.5}}$	6.303	5.206
2a	Churchill et al. (1962)	E_4	$k_2 = 0.0217\frac{u^{2.695}}{d^{3.085}s^{0.825}}$	0.563	1.044
2b		CEB	$k_2 = 5.01\frac{u^{0.969}}{d^{1.673}}$	4.227	4.382
3	Krenkel and Orlob (1963)	E_6, KO	$k_2 = 173.01\frac{(us)^{0.404}}{d^{0.66}}$	12.658	13.010
4a	Owens et al. (1964)	E_8	$k_2 = 6.91\frac{u^{0.73}}{d^{1.75}}$	9.407	8.226
4b		E_9, OEG	$k_2 = 5.35\frac{u^{0.67}}{d^{1.85}}$	8.825	7.201
5	Dobbins (1965)	DB*	$k_2 = 55.2\frac{1+Fr^2}{(0.9+Fr)^{1.5}}\frac{(us)^{0.375}}{d}\coth\left[\frac{4.75(us)^{0.125}}{(0.9+Fr)^{0.5}}\right]$	7.443	6.342
6a	Langbein and Durum (1967)	E_7	$k_2 = 5.14\frac{u}{d^{1.33}}$	3.029	3.582
6b		LD	$k_2 = 5.14\frac{u}{d^{0.67}}$	1.681	2.472
7	Issacs and Gaudy (1968)	IG	$k_2 = 4.76\frac{u}{d^{1.5}}$	3.264	3.650
8	Cadwallader and McDonnell (1969)	E_3, CM	$k_2 = 186.07\frac{(us)^{0.5}}{d}$	8.611	8.386
9	Negulescu and Rojanski (1969)	NR	$k_2 = 10.91\left(\frac{u}{d}\right)^{0.85}$	5.419	6.856
10	Thackston and Krenkel (1969)	TK*	$k_2 = 24.9\frac{u^*(1+Fr^{0.5})}{d}$	0.813	1.140
11	Padden and Gloyna (1971)	PG	$k_2 = 4.53\frac{u^{0.703}}{d^{1.054}}$	3.473	3.758
12a	Bennett and Rathbun (1972)	E_1, BR1	$k_2 = 32.69\frac{u^{0.413}s^{0.273}}{d^{1.408}}$	10.357	8.365
12b		E_2, BR2	$k_2 = 5.58\frac{u^{0.607}}{d^{1.689}}$	8.884	7.357
13	Parkhurst and Pomeroy (1972)	PP*	$k_2 = 48.5\frac{(1+0.17Fr^2)(us)^{0.375}}{d}$	6.140	5.590
14	Bansal (1973)	BN	$k_2 = 1.81\frac{u^{0.6}}{d^{1.4}}$	2.254	2.044
15	Owens (1974)	–	$k_2 = 50.8\frac{u^{0.67}}{d^{0.85}}$[###]	14.998	17.013
16	Tsivoglou and Neal (1976)	E_{10}, TN	$k_2 = k_2{}'us$[####]	8.100	14.850

17	Smoot (1988)	SM	$k_2 = 543\frac{u^{0.5325}s^{0.6236}}{d^{0.7258}}$	8.634	9.387
18	Thackston and Dawson (2001)	TD*	$k_2 = 4.97\frac{u^*(1+9Fr^{0.25})}{d}$	0.740	1.077
19a	Raymond et al. (2012)	Rm_1	$k_{600} = 5037(us)^{0.89}d^{0.54}$	7.150	10.524
19b		Rm_2	$k_{600} = 5937(1-2.54Fr^2)(us)^{0.89}d^{0.58}$	7.965	11.520
19c		Rm_3	$k_{600} = 1162u^{0.85}s^{0.77}$	6.106	7.321
19d		Rm_4	$k_{600} = 951.5(us)^{0.76}$	6.169	7.018
19e		Rm_5	$k_{600} = 2841us + 2.02$	8.048	7.410
19f		Rm_6	$k_{600} = 929(us)^{0.75}Q^{0.011}$	6.488	7.296
19g		Rm_7	$k_{600} = 4725(us)^{0.86}Q^{-0.14}d^{0.66}$	8.115	13.108

#: Average stream depth and flow velocity are taken from (Table 1). The average shear velocity, u_*, computed as $u_* = u(C_D)$ with C_D being the drag coefficient (Wüest and Lorke 2003). An average C_D of 3.3 x 10^{-3} was used for both sites based on fi surveys of the River Avon sub-catchments (Rovelli et al. 2017). The average slope, 0.002 m m^{-1}, was estimated from GPS measurements during the respective field campaigns.

##: Reference equation numbers and abbreviations from Aristegi et al. (2009) and Palumbo and Brown (2014), respectively.

###: This equation requires depth in cm and flow velocity in cm s^{-1}.

####: with k_2' being 31183 s m^{-1} d^{-1} for Q < 0.280 m^3 s^{-1} and 22500 s m^{-1} d^{-1} for Q > 0.280 m^3 s^{-1}, respectively (Palumbo and Brown 2014).

*: These equations were identified to be the most suited (i.e., top performer) for the site mean depth and flow based on the suggestions of Palumbo and Brown (2014).

Supporting Figures

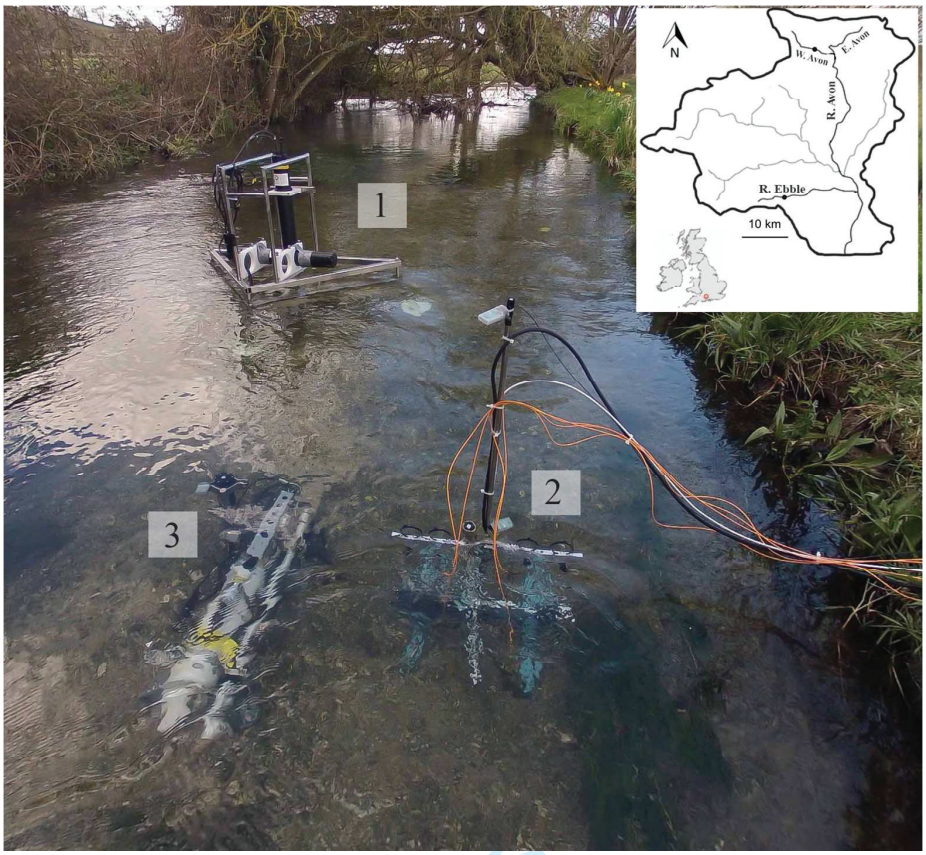

Figure S1. Catchment of the Upper River Avon and field measurement setup in the River Ebble (UK). The instruments consisted of [1] an aquatic eddy co-variance module, [2] a water column incubation stand, and [3] a CTD logger, which was also equipped with a PAR sensor and an O_2 optode. The setup also included riparian piezometers and a meteorological station (*see* Heppell et al., 2017). Dots on the catchment maps indicate the investigated reaches on the rivers Ebble (CE) on the Chalk, and West Avon (GA) on the Greensand.

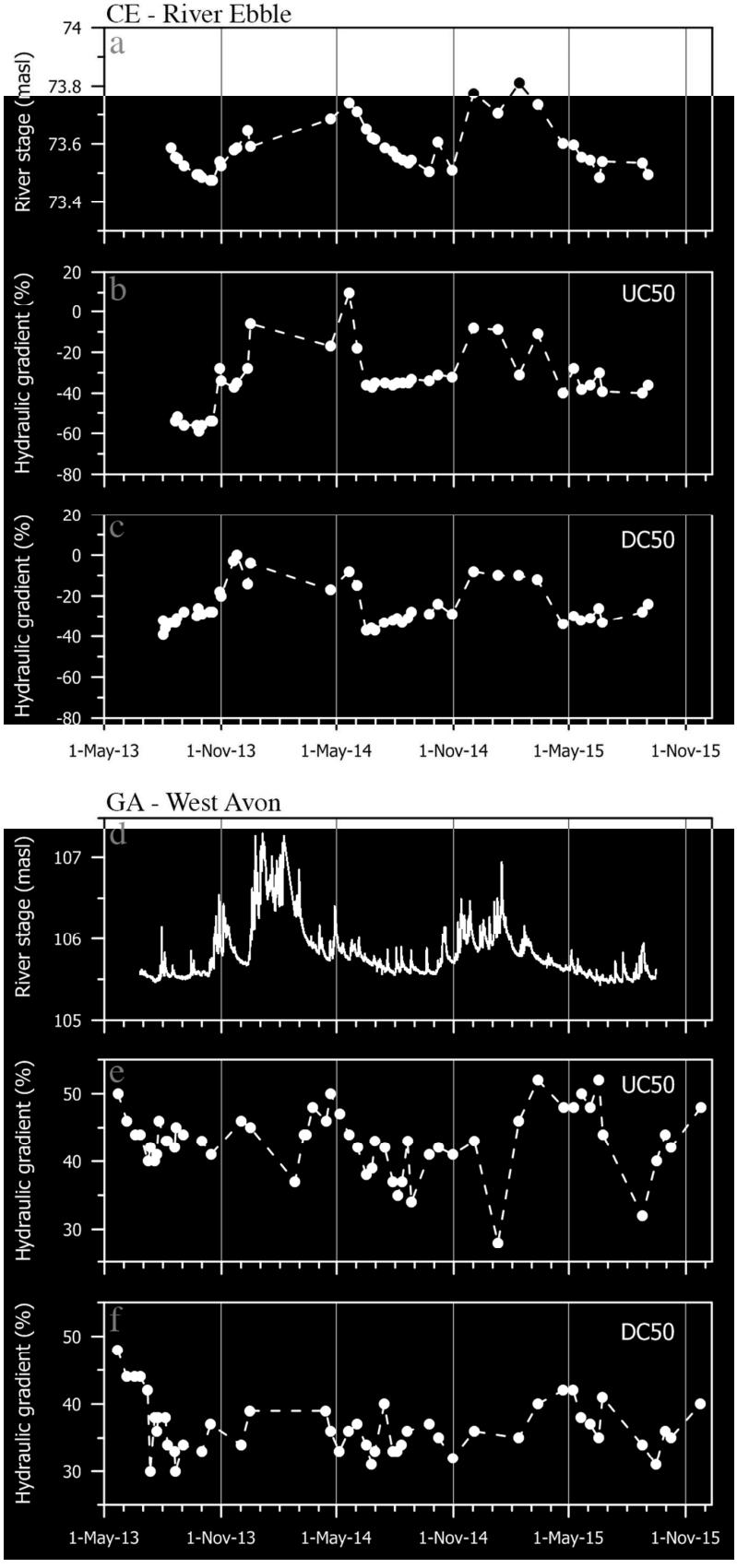
CE - River Ebble
a
River stage (masl)
74
73.8
73.6
73.4
b
UC50
Hydraulic gradient (%)
20
0
-20
-40
-60
-80
c
DC50
Hydraulic gradient (%)
20
0
-20
-40
-60
-80
1-May-13
1-Nov-13
1-May-14
1-Nov-14
1-May-15
1-Nov-15
GA - West Avon
d
River stage (masl)
107
106
105
e
UC50
Hydraulic gradient (%)
50
40
30
f
DC50
Hydraulic gradient (%)
50
40
30
1-May-13
1-Nov-13
1-May-14
1-Nov-14
1-May-15
1-Nov-15

Figure S2. Stream stage and groundwater hydraulic gradient at the rivers Ebble (CE; a–c) and West Avon (GA; d–f). The hydraulic gradient was determined from in-stream 50 cm deep piezometers 10 m apart, upstream (UC50) and downstream (DC50), from dipped levels. Positive gradients indicate groundwater upwelling, i.e. a net inflow of groundwater into the stream, while negative gradients indicate downwelling, i.e., a net loss of water from the stream to the aquifer. Estimates for spring 2013 were assumed to be equal to the same period in 2014, as mean seasonal gradients were found to be comparable across consecutive years. Stage plot for CE (a) are based on dips, while GA stage time series (d) was obtained at 15-min interval from a pressure logger (HOBO pressure transducer; Onset, USA) installed in the piezometer.

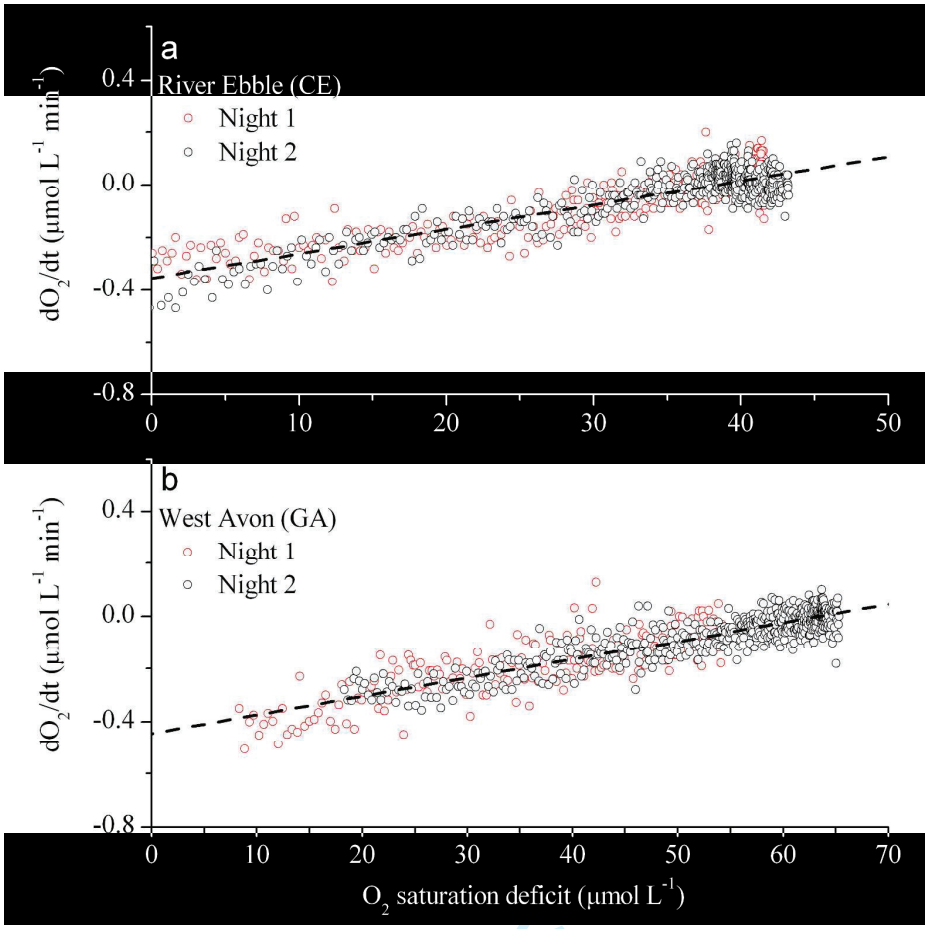

Figure S3. Nighttime regression (NR) method applied to in-stream measurements of O_2 at the rivers (a) Ebble (CE) and (b) West Avon (GA). The dashed line indicates the linear regression fitted through both night's data combined, with the slope representing the nighttime gas exchange coefficient (k_{NR}) and the intercept representing nighttime respiration. Values of k_{NR} and associated regression coefficients, R^2, are presented in Table 2. Note that no statistically significant ($p<0.05$) difference was observed between k_{NR} from night 1 and 2 at GA, while k_{NR} values at CE were statistically different, but within <10%.

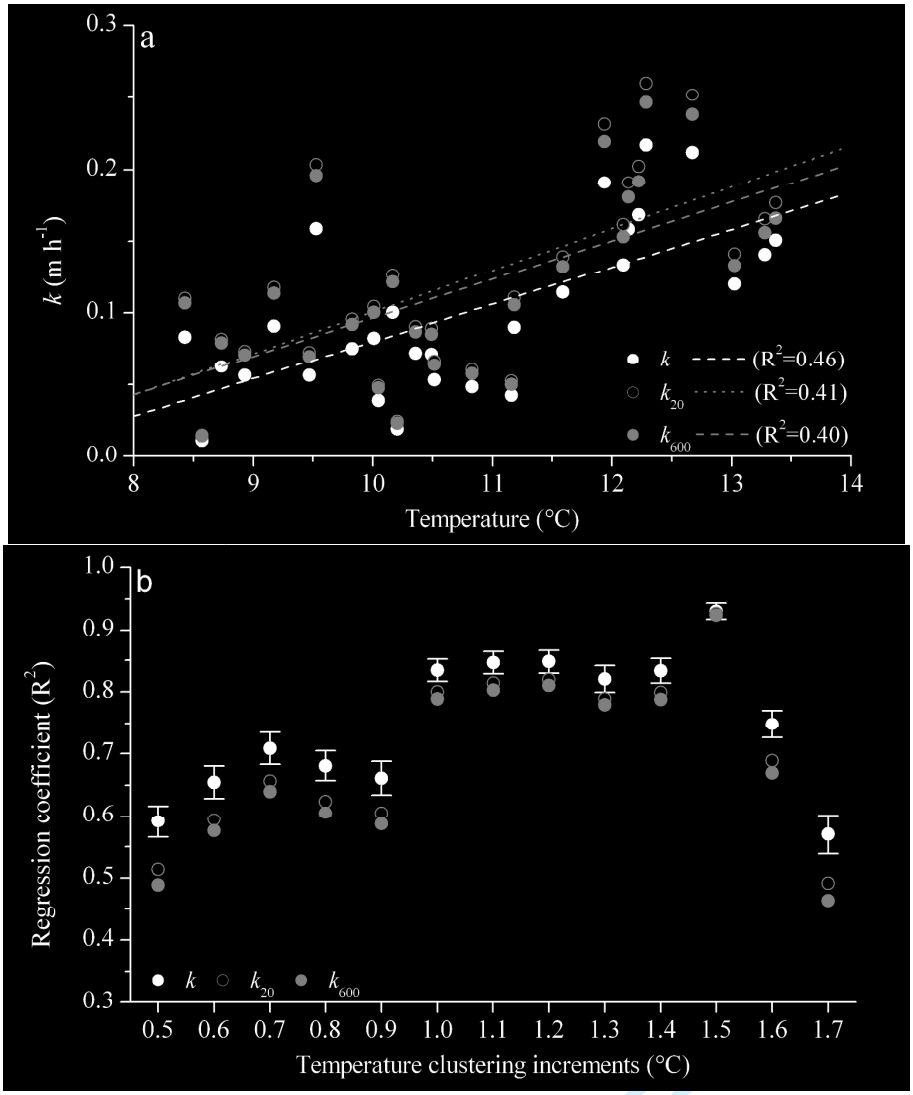

Figure S4. Temperature dependencies of the gas transfer velocity k at river Ebble (CE). (a) Local gas transfer velocity, k, and k standardized to 20°C (k_{20}) and to a Schmidt number of 600 (k_{600}) as a function of temperature. (b) Effect of temperature clustering increments on the relationship between temperature and local oxygen gas transfer velocity, k, and for k standardized to 20°C (k_{20}) and to a Schmidt number of 600 (k_{600}). For each increment, only clusters with $n \geq 3$ were considered usable for analysis by linear regression, to ensure that sparse single data points or data pairs would not bias the relationship; similarly, only increments with at least 4 data clusters were further considered for the regression analysis. The highest correlation ($R^2>0.9$) was obtained by clustering temperature in 1.5 °C increments. The standard deviation bars of R^2 values were comparable in size for k, k_{20} and k_{600}, but are only shown for k.

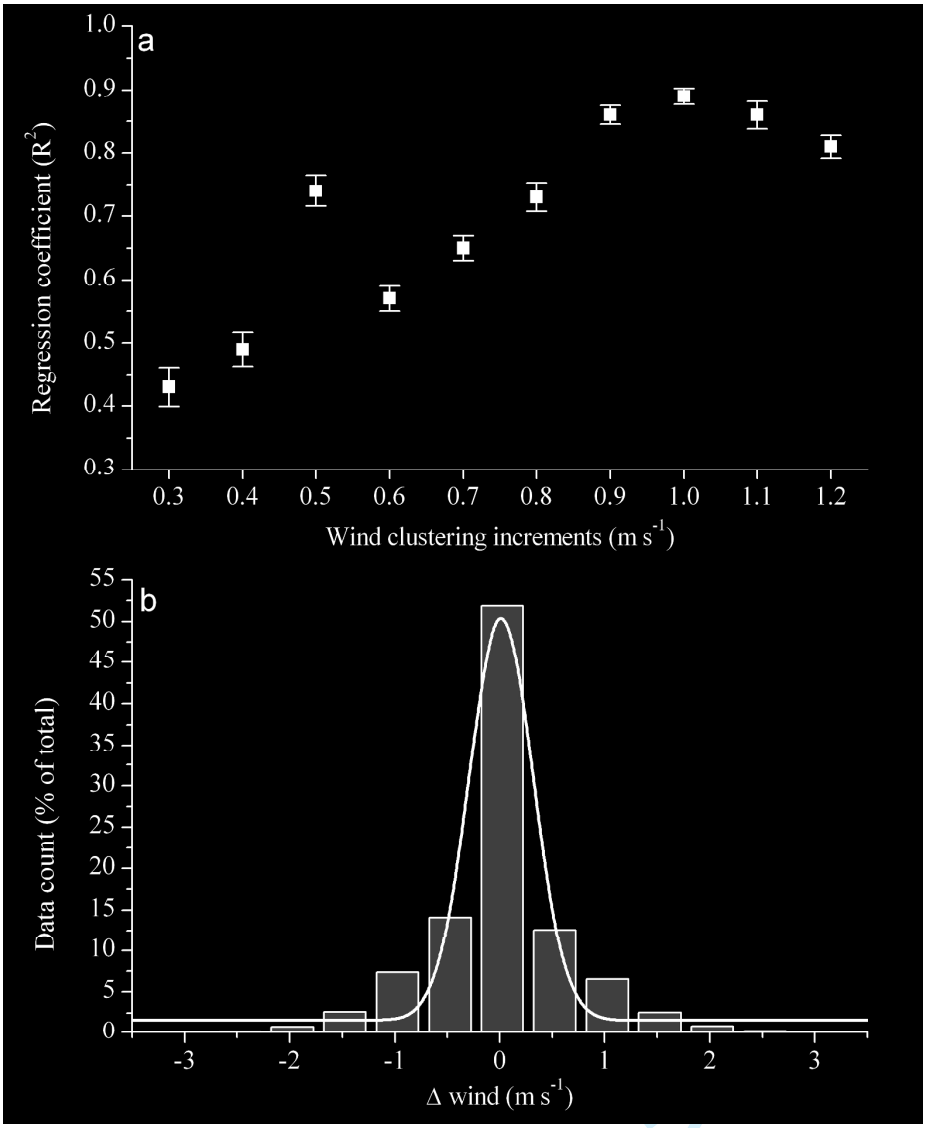

Figure S5. (a) Effect of wind clustering increments on the relationship between wind speed (m s^{-1}) and the standardized oxygen gas transfer velocity to a Schmidt number of 600 (k_{600}). For each increment, only clusters with $n \geq 3$ were considered suitable for analysis by linear regression, to ensure that sparse single data points or data pairs would not bias the relationship; similarly, only increments with at least 4 data clusters were further considered for the regression analysis. Note that the highest correlation was obtained by clustering wind dynamics in 1 m s^{-1} increments. Error bars indicate the standard deviation of R^2. (b) Frequency count analysis on combined wind measurements at river Ebble (CE) and West Avon (GA). Based on a Gaussian distribution curve fit (R^2=0.97), >90% of the wind fluctuations were within ±1 m s^{-1}.

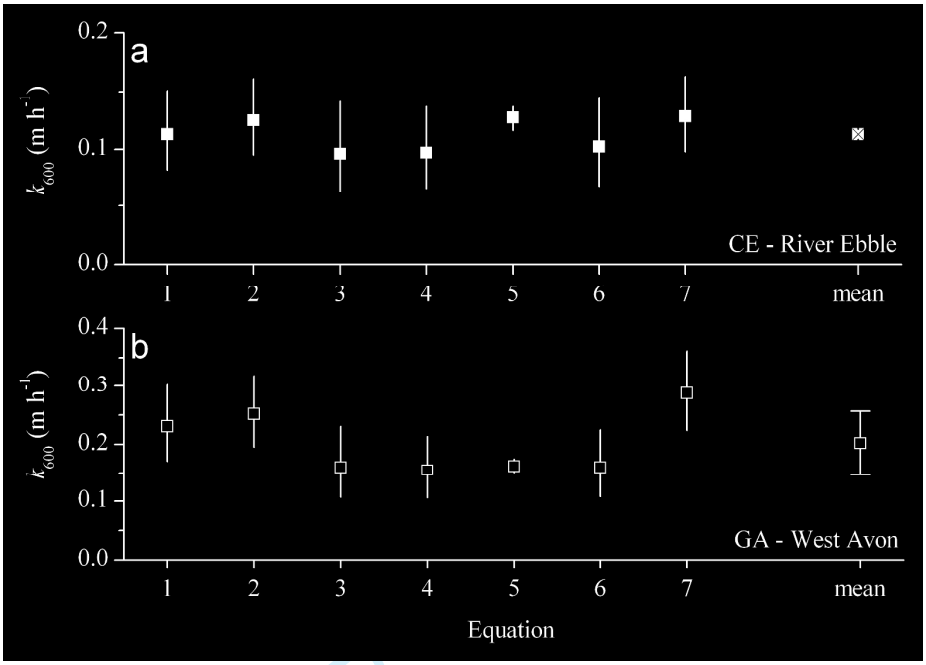

Figure S6. Prediction of gas transfer velocity (k_{600}) for (a) River Ebble (CE) and (b) West Avon (GA) based on each streams' hydraulic properties and the equations provided by Raymond et al. (2012). Error bars on each equation represent the statistical range of the estimates and were obtained by accounting for the variability (i.e., standard deviation) of each parameter (*see* Raymond et al. 2012). The combined mean value ± standard deviation from all equation is also provided for comparison.